Using mass spectrometry to Measure Protein Turnover in a Midbrain Organoid model of Parkinson's Disease

Jing Dong

Degree of Master of Science
Department of Pharmacology and Therapeutics
McGill University, Montreal

December 2022

A thesis submitted to McGill University in partial fulfillment of the requirements of the degree of Master of Science

Table of Contents

Acknowledgements

Firstly, I would like to thank Dr. Jean François Trempe for his guidance, leadership, and kindness throughout my studies. I am grateful for the opportunity to work on this project and it has been a privilege to be a member of the lab. The insights derived from his lectures, meetings, and presentations has honed my passion for science and shaped the person I am today. I would also like to thank Andrew Bayne for teaching me techniques since I was an undergraduate student, helping me troubleshoot experiments, and spurring me with exciting ideas to reflect upon. Not only has Andrew been an extraordinary mentor, he has been a true friend who has supported me through tough times.

I would also like to thank Anthony Duchesne for transitioning this project to me and facilitating my onboarding. His previous work has laid the foundation to many of the analytical methods explored in this project.

I would also like to express gratitude to my committee members Dr. Terry Hébert, Dr. Paul Clarke, and Dr. Jeff Xia for their guidance and insightful questions. Thank you to Nathalie Croteau, Dr. Simon Veyron, and Dr. Shafqat Rasool for their unwavering support and encouragement. Thank you to Tara Shomali and remaining lab members for creating a fun and happy work environment.

I would like to thank Lorne Taylor's team at the MUHC Proteomics platform for the use of the mass spectrometer and their advice. I am thankful to our collaborators Dr.

Nguyen-Vi Mohamed and Dr. Meghna Mathur in the Durcan lab at Montreal Neurological Institute for the generation, growth, and development of the midbrain organoids. Thank you as well to Dr. Wei Yi in Fon Lab for assisting with the development of the organoid protein extraction protocols.

Finally, I am grateful to Parkinson's Society Canada, Michael J Fox Foundation, Healthy Brains for Healthy Lives (HBHL), and Canadian Institutes of Health Research (CIHR) for funding this project.

Abstract

Parkinson's Disease (PD) is a severe disorder characterized early in the disease by the selective death of dopaminergic neurons. Mitochondrial damage, and consequentially mitochondrial turnover is central to neuronal health and the pathogenesis of the disorder. PINK1 and Parkin are two proteins that play an essential role in mitochondrial quality control and their mutations are known to cause early-onset PD. Prior studies demonstrated that the PINK1/Parkin pathway selectively promotes the degradation of respiratory chain proteins in *Drosophila*. Yet, how this phenomenon translates to neurodegeneration and whether it is observed in other models remains unknown. Incidentally, human midbrain organoids (hMOs) recently emerged as a novel model system that holds promise to elucidate biological processes such as the PINK1/Parkin canonical pathway. Due to their scientific infancy, validated experimental methodologies to interrogate these organoids are lacking. To this end, we developed a SILAC-based approach comprised with a novel data processing pipeline to measure global protein turnover in organoids at baseline. We successfully characterized 773 protein half-lives and compared them to Parkin knock out (PKO) hMOs. Surprisingly, we found no significant differences in the turnover of mitochondrial proteins between Wild-type and PKO hMOs. Furthermore, we compared our results with previously published studies and found that hMOs half-lives correlate with mouse cortical proteins better than primary cortical neurons. In future work, we intend to analyze hMOs with all PD-related mutations to potentially uncover a unifying basis between environmental, familial, and sporadic cases. Our work sets the stage to identify new degradation pathways and components to be therapeutically targeted to improve PD patient lives.

Résumé

La maladie de Parkinson (MP) est une maladie grave caractérisée au début de la maladie par la mort sélective des neurones dopaminergiques. Les lésions mitochondriales, et par conséquent le renouvellement des mitochondries, sont au cœur de la santé neuronale et de la pathogenèse de la maladie. PINK1 et Parkin sont deux protéines qui jouent un rôle essentiel dans le contrôle de la qualité mitochondriale et leurs mutations causent une forme précoce de la MP. Des études antérieures ont démontré que la voie PINK1/Parkin favorise la dégradation sélective des protéines de la chaîne respiratoire chez la drosophile. Cependant, on ignore comment ce phénomène se traduit par la neurodégénérescence et s'il est observé dans d'autres modèles animaux. Par ailleurs, les organoïdes de mésencéphale humain (OMh) sont récemment apparus comme un nouveau système modèle prometteur pour élucider des processus biologiques tels que la voie canonique PINK1/Parkin. En raison de leur nouveauté, les méthodologies expérimentales validées pour interroger ces organoïdes font défaut. À cette fin, nous avons mis au point une approche basée sur le SILAC et un nouveau système de traitement des données pour mesurer le taux de renouvellement des protéines dans les organoïdes. Nous avons caractérisé avec succès 773 demi-vies de protéines et les avons comparées à celles des OMhs ‘knock-out’ (PKO). Étonnamment, nous n'avons trouvé aucune différence significative dans le renouvellement des protéines mitochondriales entre les OMHs de type sauvage et les OMHs PKO. De plus, nous avons comparé nos résultats avec des études publiées précédemment et nous avons constaté que les demi-vies des OMhs sont en meilleure corrélation avec les protéines corticales de la souris que les neurones corticaux

primaires. Dans nos futurs travaux, nous avons l'intention d'analyser les OMhs avec toutes les mutations liées à la MP afin de découvrir une base unificatrice entre les cas environnementaux, familiaux et sporadiques. Nos travaux vont permettre d’identifier de nouvelles voies de dégradation et de nouvelles cibles thérapeutiques pour améliorer la vie des patients atteints de la MP.

Contribution of authors

All experiments were conceptualized and planned by Dr. Jean-François Trempe, Jerry Dong, and Anthony Duchesne. This thesis was written by Jerry Dong and edited by Dr. Jean-François Trempe.

Chapter 2

Midbrain organoid generation and SILAC timecourse incubation was performed by Nguyen-Vi Mohamed and Meghna Mathur (Montreal Neurological Institute, Durcan Lab, McGill University). Wei Yi, Carol X.Q. Chen, Zhipeng You, and Narges Abdian assisted in the methodology. Midbrain organoid sample preparation and in-gel digestion was performed by Anthony Duchesne. Sample injection into the Orbitrap instrument was performed by Lorne Taylor (MUHC). Dr. Edward Fon and Dr. Thomas Durcan assisted in the conceptualization of this project. Andrew Bayne contributed to the writing, formal analysis, and assisted with the generation of figure 2.7.

I performed all remaining work including the formal analysis, data curation, validated methodologies, and investigation of the organoid data.

List of abbreviations

2D: 2-dimensional

3D: 3-dimensional

AD: Alzheimer's Disease

ATP: Adenosine 5′-triphosphate

CMA: Chaperone-mediated autophagy

CV: Coefficient of variation

D3-Leu: [5,5,5]-Deuterium-3-Leucine

DA: Dopaminergic

DDA: Data-dependent acquisition

GBA: Glucocerebrosidase

GFP: Green fluorescent protein

GO: Gene ontology

H:L: Heavy to Light ratio

hMO: Human midbrain-like organoids

IPSC: Induced pluripotent stem cells

KO: Knock out

LAMP2A: Lysosome-associated membrane protein

LC-MS/MS: Liquid Chromatography with tandem mass spectrometry

LRRK2: Leucine rich repeat kinase 2

m/z: Mass to charge

MBOs: Midbrain-like organoids

MDV: Mitochondria derived vesicles

MPTP: l-Methyl-4-phenyl-1 ,2.5.6-tetrahydro-pyridine

MQC: Mitochondria Quality Control

MS: Mass spectrometry

PD: Parkinson's Disease

PINK1: Phosphatase and tensin homolog (PTEN)-induced kinase 1

PKO: Parkin knockout

POLG: Proofreading-deficient mutation of polymerase gamma

PQC: Protein Quality Control

ROS: Reactive oxygen species

SILAC: Stable isotope labeled amino acids in cell culture

SNc: Substantia nigra pars compacta

SRM: Selected reaction monitoring

$t_{1/2}$: Half-life

Ub: Ubiquitin

UPS: Ubiquitin Proteasome System

WT: Wild-type

α-syn: alpha-synuclein

List of tables and figures

Chapter 1 Introduction

1.1 Parkinson's Disease

Parkinson's Disease (PD) manifests in four cardinal motor symptoms consisting of bradykinesia, resting tremor, rigidity, and postural instability which appears in later stage progressions (*Parkinson's Disease: Pathogenesis and Clinical Aspects*, 2018). The disease affects approximately 1% of the population over 60 years old and pivots itself as the second most common neurodegenerative disease next to Alzheimer's disease (AD) (Tysnes & Storstein, 2017). PD is characterized by the selective death of dopaminergic (DA) neurons in the substantia nigra pars compacta (SNc) located in the midbrain. A classical hallmark of the disorder is the presence of Lewy bodies, a term coined by Fritz Jacob Heinrich Lewy who discovered these structures in PD patient brains in 1912 (Holdorff, 2002). Aberrant accumulation and misfolded forms of *α*-synuclein (*α*-syn), a protein involved in the compartmentalization and recycling of neurotransmitters, is the main component of Lewy bodies (Xu & Pu, 2016). Yet, the underlying cause of how *α*-syn aggregates contribute to the specific cell death of DA neurons remains unknown. Studies have proposed that its toxic effects are implicated in pathways involved with synaptic-vesicle trafficking, mitochondrial function, endocytosis, and autophagy (B.-K. Choi et al., 2013; Cuervo et al., 2004; Martin et al., 2006; Mazzulli et al., 2011; Winslow et al., 2010). For example, α-syn is degraded through chaperone mediated autophagy (CMA), an important lysosome-dependent targeting process that may be linked to mitochondria quality control (MQC) (Yang et al., 2016). Mutants of α-syn that cause PD are poorly degraded by CMA, yet still bind to the lysosomal receptor LAMP2A preventing the degradation of other CMA substrates by the lysosome (Cuervo et al., 2004).

Additionally, α-syn can interact with dopamine non-covalently to generate a dopamine-modified form that has been shown to interfere with CMA activity and is poorly translocated in the lysosomes (Martinez-Vicente et al., 2008). This finding along with the observation that CMA inhibition is increased in DA neurons compared to cortical neurons could potentially explain the preferential loss of DA neurons in PD (Martinez-Vicente et al., 2008). Furthermore, Shahmoradian et al. have identified distorted organelles, such as mitochondria, and other membrane fragments in the composition of Lewy body inclusions in postmortem PD patient brains (Shahmoradian et al., 2019). These observations indicate that mitochondrial damage and defective organelles are also implicated in PD-affected neurons. Although, the exact mechanism of PD continues to elude the scientific community, it is clear that protein quality control (PQC) plays a central role to the pathogenesis of PD. This Introduction will emphasize mitochondrial dysfunction and impairment of autophagy/lysosomal pathways as an overarching theme of PD.

1.2 PD is linked to the mitochondria

Evidence that the mitochondria is implicated in PD was first introduced in 1989 when a group of four individuals developed severe parkinsonism, a term used to describe a broad range of symptoms observed in PD (Langston et al., 1983). This group consumed a recreational drug contaminated with a compound known as 1-methyl-4-phenyl-1,2,5,6-tetrahydropyridine (MPTP), a protoxin that is converted inside DA neurons to MPP+, which inhibits complex I of the electron transport chain. Intriguingly, rats undergo nigrostriatal degeneration when exposed to rotenone, a potent pesticide that also inhibits complex I (Sherer et al., 2003). Notably, the disruption of complex I has been shown to

alter changes in genes related to axonal growth and induce progressive parkinsonism in mice (González-Rodríguez et al., 2021).

Several theories have been proposed to explain how mitochondrial dysfunction is associated with the selective death of DA cells in the SNc. Firstly, SNc DA neurons are particularly vulnerable due to their large axonal arborization. Studies in rats demonstrate that DA neurons can make massive branches of synapses and have up to 200 000 vesicular release sites in the striatum (Matsuda et al., 2009). Bolam et al, estimates that these number of synapses put SNc DA neurons at least 2 orders of magnitude larger than its other neuronal counterparts (Bolam & Pissadaki, 2012). The consequence of these vast connective networks is that they require a higher energy demand which makes these neurons uniquely susceptible to any perturbations in oxidative phosphorylation. SNc neurons are so extreme that they are constantly operating at their maximum and any burden on the energy supply will “tip them over the edge” eventually leading to cell death. Secondly, the vulnerability of SNc DA neurons can be attributed to its autonomous pacemaking activity. They generate slow action potentials that are broad, which maximizes the entry of Ca^{2+} through distinctive L-type Cav1 Ca^{2+} channels (Surmeier et al., 2017). This differs from the physiology of DA neurons found in the ventral tegmental area (VTA), an area located in the midbrain responsible for reward and motivation (Lammel et al., 2012). The elevated intracellular Ca^{2+} imposes additional energetic burden on the neuron as it needs to sequester the Ca^{2+} by investing more resources on ATP-dependent transporters in the endoplasmic reticulum (Surmeier, 2007).

It is important to note that these features of SNc DA neurons are not intrinsically lethal to the cell but they increase their vulnerability in the face of additional stressors such as neurotoxins, elevated reactive oxygen species (ROS), damage accumulated through age,…etc. In the case of MPTP, inhibition of complex I not only reduces ATP output but it also increases the production of ROS. This leads to a vicious positive feedback loop as the generation of ROS can cause cellular damage to nucleic acids, proteins, and even the electron transport chain itself to produce more ROS (Dauer & Przedborski, 2003). Hence, it is vital that the body maintains a healthy environment by installing mechanisms to recycle dysfunctional organelles and prevent the spread of stressors such as oxidative damage. This theme of PQC continues to loom over the scientific community as investigations turn towards the genetics of PD.

1.3 PINK1/Parkin is implicated in MQC

The majority of PD cases are sporadic but some propose that approximately 5-10% of patients suffer from a monogenic form (Lill, 2016). The first familial form of PD identified is caused by an autosomal dominant mutation (A53T) in *SNCA*, which encodes for α-syn (Polymeropoulos et al., 1997). Likewise, the mutation G2019S in *LRRK2* is considered the most common, accounting for about 4% familial cases and 1% of sporadic cases (Tolosa et al., 2020). Recessive loss-of-function mutations in the proteins *PARK2*, *PINK1*, and *DJ-1* have also been identified to cause early-onset forms of PD (< 50 years). Although they account for only a small fraction of the total pool of PD cases, these genes play an essential role in shedding light on the mechanisms that underlie neurodegeneration. *DJ-1* has been shown to exhibit neuroprotective effects in DA

neurons through acting as an oxidative stress sensor further reinforcing the importance of PQC. Indeed, *PARK2 and PINK1* are also implicated in MQC. *PARK2,* which encodes for the E3 ubiquitin ligase Parkin, is the most common recessively mutated gene consisting of around 8.6% early-onset PD cases. *Drosophila* models with Parkin-null mutations exhibit reduced lifespan, locomotor defects and sterility in males (Greene et al., 2003). Likewise, PINK1-knockout *Drosophila* display a similar phenotype resulting in male sterility, muscle degeneration and morphological defects in the mitochondria (Clark et al., 2006). It is clear that PINK1 and Parkin are implicated in the MQC pathway, where PINK1 acts upstream in the process as a damage sensor and Parkin is the effector.

1.3.1 PINK1/Parkin mediated mitophagy

Mitophagy is the selective removal of mitochondria by autophagy (Tolkovsky, 2009). PINK1/Parkin is implicated in MQC through mitophagy. Briefly, when mitochondria undergo stress (such as membrane depolarization), PINK1 accumulates onto the outer-mitochondrial membrane and homodimerizes (P. Ge et al., 2020). This promotes kinase activation, allowing PINK1 to phosphorylate ubiquitin at Ser65 which in turn stimulates the recruitment of Parkin in the cytosol. Parkin will then “amplify” the detection signal through creating ubiquitin chains on various downstream substrates. The long ubiquitin chains promote the recruitment of ubiquitin adaptor proteins which lead to the engulfment of the damaged mitochondria by the autophagosome (Whitworth & Pallanck, 2017). However, this process has yet to be shown *in vivo.*

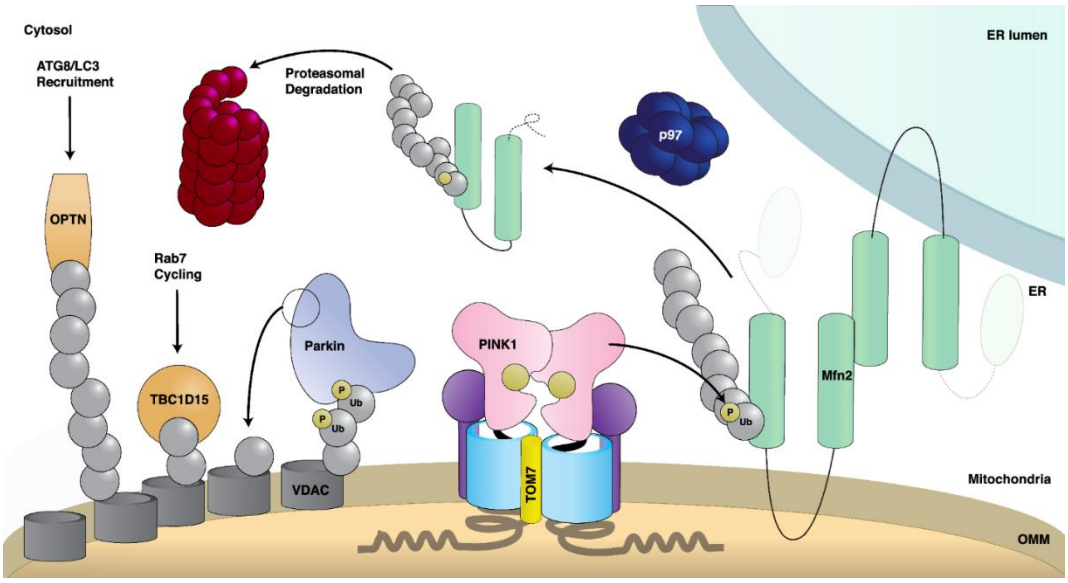

Figure 1.1: Overview of the PINK1/Parkin pathway in MQC (Bayne & Trempe, 2019)**:** OMM = Outer Mitochondrial Membrane, ER = Endoplasmic Reticulum, Ub = Ubiquitin

1.3.2 PINK1 and Parkin's protective role in MQC is multifunctional

PINK1 and Parkin's role in MQC extends beyond mitophagy. Indeed, PINK1 and Parkin can manipulate mitochondrial dynamics through facilitating fission and inhibiting fusion. For instance, Parkin ubiquitination promotes the degradation of mitofusin 1 and 2, two GTPases that mediate mitochondrial fusion (Tanaka et al., 2010; Ziviani et al., 2010). Likewise, PINK1 is able to independently activate and recruit DRP1 to promote fission in the mitochondria (Pryde et al., 2016). This process allows cells to segregate local damaged areas of the organelle by sending them off to the lysosome whilst preventing dysfunctional sections from refusion and transmitting the injury to other healthy mitochondria. Mitochondrial trafficking is also regulated by PINK1/Parkin through the destruction of Miro, a protein that connects mitochondria to microtubules (Kane & Youle, 2011). PINK1 phosphorylation of Miro leads to its degradation which detaches the

defective mitochondria from the microtubule network and prevents its transport throughout the cell. Another example of PINK1/Parkin-mediated quality control is observed in mitochondrial derived vesicles (MDVs), a structure that transports specific cargo from the mitochondria to various organelles (Soubannier et al., 2012). PINK1 and Parkin are required for the generation of MDVs that are destined for the lysosome (G. McLelland et al., 2014). This mechanism has been hypothesized to allow for the selective removal of specific regions in the organelle that experience local oxidative damage instead of removing the entire organelle, which is resource-intensive. Indeed, kinetic analyses demonstrate that the generation of Parkin-dependent MDVs occurs rapidly in response to ROS and precedes mitophagy (G.-L. McLelland et al., 2014). Sugiura et al characterizes MDVs as a likely first line defense in MQC and highlights the importance of cargo selection in protecting the cell from oxidative damage (Sugiura et al., 2014). Indeed, MDVs generated in response to mitochondrial stress are enriched in oxidized protein and cargo in brain MDVs were significantly enriched with proteins involved in oxidative phosphorylation (Roberts et al., 2020; Soubannier et al., 2012).

It is clear that PINK1/Parkin activation is instrumental to MQC and its genetic ablation causes the loss of DA neurons in humans. Emerging evidence present mitochondrial dysfunction and impaired autophagy as potential unifying themes surrounding the pathogenesis of familial, environmental and sporadic cases of PD (Ryan et al., 2015). However, the impairment of mitochondria across all patients with PD is unlikely to occur by the same mechanism and the PINK1/Parkin pathway's contribution to non-familial cases is unclear. A number of questions remain: What is PINK1/Parkin's true role in global

mitophagy at baseline? To what degree does PINK1/Parkin inactivation contribute to the pathogenesis of sporadic PD? Are there any other players that are implicated in MQC yet to be discovered? Interestingly, mitochondrial proteases have also emerged as key regulators of reshaping the proteome and overseeing MQC. Notably, mitochondrial hyperpolarization has been shown to activate m-AAA proteases through the degradation of TMBIM5 to breakdown complex I and confine the spread of ROS to hyperpolarized mitochondria (Patron et al., 2022). The regulation of proteolytic activity is also likely to be central towards pathological condition. Thus, the jury is still out for identifying the precise targets and pathways that are perturbed in PD. Performing proteome wide protein turnover studies will shed light on PQC mechanisms such as mitophagy and proteolysis which could provide a unifying basis for PD and expand our understanding of neuronal vulnerability.

1.4 PQC through the lens of protein turnover

Quality control encompasses various molecular processes that involve import, surveillance, folding, and turnover of proteins. Protein turnover – the renewal and replacement of decaying proteins with the synthesis of new functional proteins – is essential for maintaining homeostasis in the cell. Ranging from minutes to several months, the turnover rate of a protein varies by its function and localization (Buscham et al., 2019; Price et al., 2010). The regulation of protein turnover is critical to not only neuronal health but is implicated in various processes such as cellular development and growth, transcription, immune response, and cell signalling (Balch et al., 2008; DeMartino & Slaughter, 1999). Pathological states can arise when this regulation is impaired. For

example, the human papillomavirus is responsible for the development of warts, cervical carcinoma, and certain head and neck cancers (Hanna et al., 2018). The virus proliferates through the production of a protein that stimulates the degradation of p53, an essential protein involved in tumor suppression (Martinez-Zapien et al., 2016; Scheffner et al., 1993). Hence, the half-life of specific proteins is often altered in pathological disease states. Measuring global turnover rates allows for the identification of these proteins or pathways that are dysregulated.

Two main degradation pathways are autophagy and the ubiquitin proteasome system (UPS). Impairment of either pathway has been shown to be associated with diseases including cancers, cardiovascular disorders, and neurodegenerative disorders(Herrmann et al., 2004; Lehman, 2009; Nemchenko et al., 2011; Nixon, 2013; White, 2015). Studies in mice show that the deletion of ATG7, a gene essential for autophagy, has been linked to PD-related phenotypes such as neurodegeneration, locomotor impairments, and accumulation of α-syn in presynaptic terminals (Friedman et al., 2012; Sato et al., 2018). Likewise, a significant decrease in proteasome activity has been observed in the hippocampus of postmortem-interval autopsied brains of patients with AD (Keller et al., 2000). Identifying drugs that can modulate these degradation pathways to restore their function is a promising therapeutic strategy.

However, before treatments can be developed to target these pathways, it is important to first measure the half-lives of healthy cells at baseline to establish a reference point. These half-lives can then be used to compare with the protein half-lives of diseased cells

to observe whether the turnover rate have been up or down-regulated. How does one then measure protein half-lives in cells?

1.4.1 Measuring protein turnover

Some of the first protein metabolism studies conducted over 80 years ago showed proof that proteins were not static and animal tissues could indeed degrade and synthesize proteins (Foster et al., 1939). The experiment involved heavily restricting the diets of rats and then administering isotopic ammonia and measuring its presence. From there, both historical and modern protein turnover studies employ an assembly of techniques that involve introducing a “tracer” into an organism of interest and measuring its change. This tracer takes the form of radioactive, biochemical, or stable-isotope label and is typically administered through the metabolism of carbon, nitrogen, or the amino acids of cells. However, high radioactive doses emitted by the tracer can harm the cell and genetically engineered tracers can disrupt the function of the tagged protein and only allows one protein to be investigated at a time. Hence, amongst these methods, Stable Isotope Labeling of Amino Acids in Cell Culture (SILAC) or in mammals (SILAM) combined with quantitative mass spectrometry emerged as the least disruptive and most comprehensive technique for conducting protein turnover experiments.

Principally, SILAC experiments involves growing two populations of cells or animals with two distinct media. The first population is exposed or fed to the “light” media containing amino acids with the natural isotope. The second population is exposed to the “heavy” medium consisting of a stable-isotope labelled amino acid which acts as a tracer.

Subsequent digested peptides that contain this tracer will include a mass shift distinguishable by MS. For example, peptides that contain the stable-isotope label [5,5,5]-^{2}H-3-leucine will contain a mass shift of 3 Da compared to peptides with standard leucine. Essential amino acids are used as tracers to ensure proper incorporation into newly synthesized proteins in the cells.

The addition of the “heavy” tracer can be thought as “pulsing” the organism to “chase away” amino acids with the natural isotope abundance to be replaced by the SILAC label. Over the course of time, cells will continuously incorporate the heavy tracer and a “heavy” to “light” (H:L) tracer ratio for each peptide in the cell can then be measured at different time points. The average of all H:L ratios for all peptides of a given protein can be used to calculate a half-life for a specific protein. This concept essentially measures the protein turnover rate through measuring the rate of “heavy” tracer incorporation into newly synthesized peptides as shown by **Figure 1.2**.

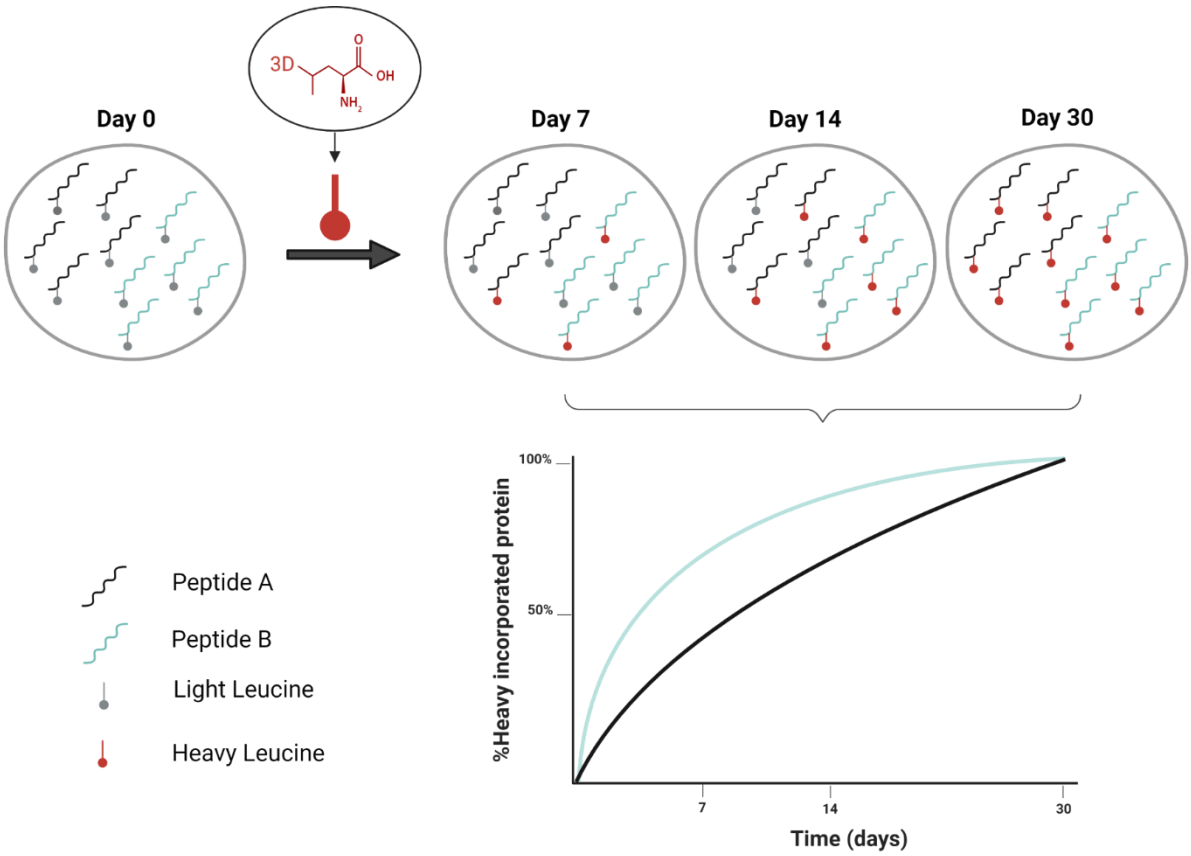

Figure 1.2: Principles of SILAC. Schematic demonstrating peptides derived from two theoretical proteins (A and B) with different half-lives incorporating the labelled tracer at separate time points. Protein B is turned over faster than protein A as it reaches a higher tracer percentage at each time point. From the tracer percentages, a half-life for each given protein can be computed.

There are a few points of caution with using SILAC to measure protein turnover. Firstly, these measurements are functioning under the assumption that the cells or animals are in a steady state throughout the course of the labeling experiment (ie. the organism is not continuously growing). At steady state, the rate of protein synthesis is equal to the rate of protein degradation and thus the global protein levels remain unchanged. Throughout dynamic processes such as cellular growth or stress response, protein production rates or degradation rates can be up or down-regulated in response to stimuli. Hence, SILAC measurements of an organism undergoing dynamic change would only be capturing

differences in synthesis or degradation rates rather than its actual protein turnover. Secondly, when a tracer is first introduced to a cell, it is diluted by unlabelled amino acids found as free amino acids or generated by the breakdown of pre-existing proteins (Hsieh et al., 2012). Hence, the amino acid pool contributing to newly synthesized protein contains a mixture of both unlabelled and labelled amino acids that must be accounted for.

1.4.2 Prior studies on mitochondrial turnover

Although the PINK1/Parkin pathway has been well established in cell cultures, evidence of its role in mitophagy *in vivo* is limited. Several studies have analyzed mitochondrial protein turnover using SILAC-based approaches and fluorescence reporters *in vivo.*

Vincow et al. first interrogated the role of the PINK1/parkin pathway through proteome-wide turnover measurements in *Drosophila* (Vincow et al., 2013a). These results were obtained through SILAC time course experiment (described in the previous section of the Introduction) using tri-deuterated leucine as a tracer label. Their findings highlight that Parkin knockout (PKO) flies displayed slower turnover for a subset of mitochondrial proteins. Intriguingly, they also observed that turnover of specific subunits in the electron transport chain experienced significantly greater impairment than ATG7 mutant flies. This suggests that Parkin selectively degrades proteins involved in oxidative phosphorylation as opposed to widespread non-specific mitophagy. If true, this could be a potential explanation for the complex I deficits and the increased susceptibility to ROS damage seen in PD (Mortiboys et al., 2008; Palacino et al., 2004; Shoffner et al., 1991).

However, other studies show seemingly conflicting results regarding PINK1/Parkin's role on mitophagy. Lee et al. assessed mitophagy through the use of a *mito*-QC reporter, a construct made of a mitochondrial targeting sequence from the OMM protein Fis1 fused with a tandem mCherry-GFP tag (Lee, Sanchez-Martinez, Zarate, et al., 2018). When exposed to the neutral pH of the cytosol, *mito*-QC fluoresces both green and red, but GFP is quenched when introduced to an acidic environment such as the lysosome which then fluoresces only red (McWilliams et al., 2016). Another tool used to measure mitophagy employs a mitochondrial-targeted form of keima, a coral-derived acid-stable fluorescent protein that emits different-colored signals at acidic and neutral pHs (Sun et al., 2015a). This tool is coined as Mt-Keima and is directed to the mitochondrial matrix through using a mitochondrial targeting sequence from COX8A (Sun et al., 2015b). Principally, fluorescent reporters measure mitophagy through using the pH sensitivities of both mito-QC and mt-Keima to distinguish free mitochondria from mitochondria in lysosomes. Lee et al generated transgenic *Drosophila* expressing these fluorescent reporters and compared mitochondrial turnover in wild type, PINK1, and PKO mutants (Lee, Sanchez-Martinez, Zarate, et al., 2018). Surprisingly, they discovered that loss of PINK1 and Parkin function had no substantial influence on basal mitophagy. Likewise, McWilliams et al also demonstrated that PINK1 knockout mice displayed no differences in basal mitophagy compared with their wild-type counterparts (McWilliams et al., 2018a). However, Liu et al detected a two-fold increase in PINK1/Parkin mitophagy from mice subjected to exhaustive exercise through mt-Keima, but not mito-QC (Y.-T. Liu et al., 2021). Evidently, fluorescent reporters present an exciting opportunity to study *in vivo* mitophagy but are not free of limitations. One drawback of fluorescence reporters is

that they do not measure the half-life of different proteins and fail to identify the degradation patterns of specific regions within the mitochondria. It is apparent that fluorescence reporters do not capture all turnover events in the cell. Further inspection of global protein dynamics is required to elucidate the PINK1/Parkin canonical pathway.

All these studies highlight the feasibility and demand for more research surrounding mitophagy. Studies need to be conducted in models that accurately reflect the physiology of PD in order to develop effective treatments. Yet, mitochondrial protein turnover has never been investigated in a mammalian model of PD to date. This manuscript aims to address that data gap.

1.5 Organoids as a novel model of PD

Organoids are 3-dimensional (3D) self-assembling tissue constructs that have the potential to recapitulate the architecture and function of an organ (Takebe & Wells, 2019). These models can be patient-specific as organoids can be derived from embryonic stem cells or obtained through the dissociation of adult organs. Due to their remarkable ability to mimic complex cellular features, human brain organoids have emerged as a novel technology to dissect neurological development and diseases (Qian et al., 2019). For example, cerebral organoids were observed to display premature neuronal differentiation in patients with microcephaly, a disorder that is notoriously difficult to capture in mouse models (Lancaster et al., 2013). Brain organoids have also identified therapeutic targets against disorders such as autism-spectrum disorder, neuro-infections. Alzheimer's

Disease, and Miller-Dieker syndrome (Dang et al., 2016; Iefremova et al., 2017; Mariani et al., 2015; Raja et al., 2016).

Recently, human midbrain-like organoids (hMOs) generated from induced pluripotent stem cells presents an exciting opportunity for modelling PD (N.-V. Mohamed et al., 2021). hMOs produce neuromelanin-like granules, a by-product of dopamine synthesis, that are chemically identical to those isolated from human SNc tissue (Jo, Xiao, Sun, Cukuroglu, Tran, Göke, Tan, Saw, Tan, & Lokman, 2016). This feature is not captured in 2D neuronal cell cultures. Furthermore, hMOs harboring *SNCA* triplication capture key features of PD expressing elevated α-syn levels and age-dependent increase in α-syn aggregation (N.-V. Mohamed, Sirois, et al., 2021b).

It is clear that hMOs holds promise as an exciting tool that can potentially complement existing *in vitro* systems in investigating PQC and neurodegeneration. Despite this, validated experimental methods to study these models are lacking and mitochondrial protein turnover has never been reported in organoids.

1.6 Rationale and research objectives

This literature review has outlined several key principles. First, PD is intimately connected with PQC. Abhorrent protein aggregation, respiratory chain deficits and increased oxidative damage observed in PD patients pivots mitochondrial dysfunction and autophagy as a central theme to the etiology of the disease. Second, PINK1/Parkin is implicated in MQC through mitophagy and other mechanisms. Interrogating this pathway holds promise to revealing pathogenic overlap between familial, environmental, and

sporadic forms of PD. Third, proteome wide turnover measurements can be used to assess PQC. For example, Vincow et al. uses a SILAC-labelling time course approach to demonstrate that Parkin-null *Drosophila* display impaired turnover in selective subunits involved in oxidative phosphorylation. This knowledge can then shed light on specific components or pathways that are dysregulated in a diseased model which can then be targeted therapeutically. However, physiologically relevant models are required to fully realize this potential. Finally, hMOs emerge as a novel PD model to address this problem. Organoids mimic the structural complexity of organs serving as a bridge between 2D cultures and *in vivo* models. However, whether hMOs live up to becoming truly powerful models of diseases or simply remain as a tool with scientific potential has yet to be proven as validated methods to study this technology is limited.

Hence, the objectives of this project are to establish a method to measure protein turnover in hMOs, as a way of determining the impact of PD mutations on mitochondrial turnover. The project has three key aims. First, to design a standardized workflow to measure protein turnover rates in hMOs. Second, to develop a robust statistical framework to validate the protein half-life calculations. Third, to apply the method to different genetic cell lines to compare turnover rates across genotypes.

To measure protein turnover, we employed a SILAC-based time course approach using D3-leucine as a tracer. hMOs were grown in triplicates across five different time points. The organoids were processed through in-gel digestion and peptides were identified through LC-MS/MS. A data processing pipeline was established to convert peptide H:L

tracer ratios to protein half-lives. This involved open-source software such as Maxquant, Skyline, and Topograph. The data processing workflow and accuracy of the protein half-lives were validated through conducting a Monte-Carlo simulation and comparing protein half-lives with previously characterized turnover rates. To determine if the method could be applied to compare genotypes, a PKO midbrain-like organoids (MBOs) was generated through introducing an exon 6 deletion in the PARK2 gene (X.-Q. Chen et al., 2022). Our results successfully and accurately identified the half-lives of 773 proteins for the first time in hMOs. These findings are reported in a research article published in the journal "Methods" for a special issue entitled "Tools for drug discovery and disease modelling".

Chapter 2: An approach to measuring protein turnover in human induced pluripotent stem cell organoids by mass spectrometry

An Approach to Measuring Protein Turnover in Human Induced Pluripotent Stem Cell Organoids by Mass Spectrometry

Jing Dong[1,5], Anthony Duchesne[1,5], Andrew N. Bayne[1,5], Nguyen-Vi Mohamed[2], Wei Yi[2], Meghna Mathur[2], Lorne Taylor[3], Carol X.Q. Chen[2], Zhipeng You[2], Narges Abdian[2], Edward Fon[2], Thomas M. Durcan[2], Jean-François Trempe[1,3,4,6,*]

[1] Department of Pharmacology & Therapeutics and Centre de Recherche en Biologie Structurale, McGill University, 3655 Promenade Sir William Osler, Montreal, Quebec, H3G 1Y6, Canada.

[2]Early Drug Discovery Unit (EDDU), Montreal Neurological Institute-Hospital, Department of Neurology and Neurosurgery, McGill University, 3801 University Street, Montreal, Quebec, H3A 2B4, Canada

[3] Proteomics Platform, Centre for Translational Biology, Research Institute of the McGill University Health Centre, 1001 Bd Décarie, Montréal, Quebec, H4A 3J1, Canada

[4] Brain Repair and Integrative Neuroscience (BRaIN) Program, Centre for Translational Biology, Research Institute of the McGill University Health Centre, 1001 Bd Décarie, Montréal, Quebec, H4A 3J1, Canada

[5] All three authors contributed equally to this work

[6] Lead contact

* Correspondence: jeanfrancois.trempe@mcgill.ca

Abstract

Patient-derived organoids from induced pluripotent stem cells have emerged as a model for studying human diseases beyond conventional two-dimensional (2D) cell culture. Briefly, these three-dimensional organoids are highly complex, capable of self-organizing, recapitulate cellular architecture, and have the potential to model diseases in complex organs, such as the brain. For example, the hallmark of Parkinson's disease (PD) – proteostatic dysfunction leading to the selective death of neurons in the substantia nigra -- present a subtle distinction in cell type specificity that is lost in 2D cell culture models. As such, the development of robust methods to study global proteostasis and protein turnover in organoids will remain essential as organoid models evolve. To solve this problem, we have designed a workflow to reproducibly extract proteins from brain organoids, measure global turnover using mass spectrometry, and statistically investigate turnover differences between genotypes. We also provide robust methodology for data filtering and statistical treatment of turnover data. Using human midbrain organoids (hMO) as a model system, our method accurately characterized the half-lives of 773 midbrain proteins. We compared these half-lives both to Parkin knockout hMOs and to previously reported data from primary cell cultures and *in vivo* models. Overall, this method will facilitate the study of proteostasis in organoid models of human disease and will provide an analytical and statistical framework to measure protein turnover in organoids of all cell types.

2.1 Introduction

2.1.1 Organoids as a novel model to recapitulate neurodegenerative disease

Three dimensional (3D) human brain organoids derived from induced pluripotent stem cells (iPSCs) have emerged as a novel tool in modelling distinct regions of the brain and can even reconstitute neuronal crosstalk via organoid fusions (Bagley et al., 2017; A. Chen et al., 2020; Jo, Xiao, Sun, Cukuroglu, Tran, Göke, Tan, Saw, Tan, Lokman, et al., 2016; Kelava & Lancaster, 2016). This technology serves as a critical bridge between 2D cultures and *in vivo* models for examining complex neural mechanisms and their dysregulation in disease. Unlike traditional *in vitro* cultures, the architecture of organoids consists of multiple region-specific cell types conferring more physiologically relevant characteristics (Fatehullah et al., 2016; N.-V. Mohamed, Sirois, et al., 2021a). Two examples of disease-relevant hallmarks in organoids that remain poorly captured in 2D culture models are: (1) midbrain organoids produce neuromelanin-like granules, a byproduct of dopamine synthesis that are highly enriched in the midbrain neurons lost in Parkinson's disease (PD) (Jo, Xiao, Sun, Cukuroglu, Tran, Göke, Tan, Saw, Tan, Lokman, et al., 2016; N.-V. Mohamed et al., 2021); (2) β-amyloid plaques and neurofibrillary tangles are also found in cerebral organoids, a pathological marker of Alzheimer's disease (AD) pathology (S. H. Choi et al., 2014).

These findings demonstrate that brain organoids complement existing model systems as a tool to study the mechanisms underlying neurodegenerative diseases. However, despite their promise as a driver for scientific discovery, the technology is still in its infancy as validated experimental methods to study these models are lacking.

2.1.2 Protein Dynamics in Neurodegeneration

Turnover - the dynamic balance of protein degradation and synthesis - is essential to maintain the homeostasis of all cells including neurons (Fecto et al., 2014). Studies have shown that dysfunctional mitochondria and their impaired turnover is a fundamental problem associated with specific neurodegenerative disorders such as PD, AD, and Amyotrophic Lateral Sclerosis (Karbowski & Neutzner, 2012). In fact, mutations in PINK1 and Parkin, two proteins implicated in the selective turnover of mitochondria, cause autosomal recessive juvenile PD (Narendra & Youle, 2011). Furthermore, defects in both the ubiquitin proteasome system and autophagy machinery lead to protein misfolding and aggregation, a common mechanism of pathogenesis in neurodegenerative diseases, such as PD, AD and Huntington's Disease (Dennissen et al., 2012; Son et al., 2012). As such, the proteome-wide study of protein dynamics in organoids presents a unique opportunity to uncover novel mechanisms underlying neurodegeneration and cell-type specificity in disease. Other studies have used quantitative mass spectrometry to profile differential protein expression in brain organoids following drug treatment; (Dakic et al., 2017; Notaras et al., 2021) however, there are currently no established methods to measure protein turnover in these systems. Our study aims to address this gap.

2.1.3 Measuring protein turnover in organoids using SILAC

Protein turnover can be measured using stable isotope labelled amino acids (SILAC) coupled with quantitative mass spectrometry (MS). While stable isotope labels can be introduced into proteins either metabolically, chemically, or enzymatically, this study will focus on metabolic labelling, as it is the most effective implementation for *in-* and *ex- vivo*

systems (Ong & Mann, 2005). Briefly, the SILAC metabolic labelling approach involves growing cells in two separate media: (1) the “light” medium, which contains an amino acid with all atoms at their natural isotope abundance and (2) a “heavy” medium, which contains heavy isotope labels incorporated into the same amino acid. The “heavy” labeled amino acid is subsequently incorporated into newly synthesized proteins, which induces a small mass shift in the digested peptides that is distinguishable by MS. The ratio of heavy to light (H:L) abundance of each peptide can be measured at different time-points in a pulse-chase-like time course experiment. The H:L ratios for all peptides of a given protein can then be averaged to compute a half-life for that particular protein. One critical requirement for the measurement of turnover in this manner is that the protein levels must remain constant throughout the time course (steady state); in this case, the rate of synthesis must equal the rate of degradation, allowing the turnover rate to be calculated.

Common SILAC labels contain ^{13}C or ^{15}N isotopes within Arg or Lys in media to 2D cell culture systems, or in heavy labelled food of animals such as zebrafish, newts and mouse. (Andersen et al., 2005; Krüger et al., 2008; Looso et al., 2010; Ong et al., 2003; Westman-Brinkmalm et al., 2011). $^{13}C_6$-labeled Lys, an essential amino acid, has been used to measure the turnover of proteins in mice (Fornasiero et al., 2018). Alternatively, leucine is also an essential amino acid that is highly abundant, and less costly than its Lys/Arg label counterparts. Furthermore, leucine does not undergo metabolic scrambling, the process in which the heavy label is metabolized and incorporated into other amino acids potentially confounding analysis (Duan et al., 2016). Leucine is catabolized in the cell to α-ketoisocaproic acid and β-hydroxy-β-methylbutyric acid, two metabolites that enter

cholesterol biosynthesis or the citric acid cycle via acetyl-CoA, where the branched aliphatic δ carbons are excreted through carbon dioxide. Leucine metabolism has indeed been observed in both astrocytes and neurons derived from human iPSCs (Salcedo et al., 2021).

Other studies have validated the use of heavy leucine in turnover measurements by feeding *Drosophila melanogaster* [5,5,5]-deuterium-3-leucine (D3-Leu) food that was incorporated into the flies over time (Vincow et al., 2013b). Likewise, organoid models can be cultured with ^{13}C,^{15}N-labeled lysine and arginine to characterize growth and protein abundance under different conditions (Gonneaud et al., 2016). Refining these organoid-specific SILAC protocols will be especially useful as the number of validated organoid genotypes and relevant disease models expand. In this work, we provide a robust methodology to measure protein turnover in iPSC-derived organoids and compare differences across cell lines. A brief experimental overview is outlined in Figure 2.1. As a test case, we compare wild type (WT) hMOs to Parkin KO (PKO) hMOs, demonstrating adequate sensitivity of our method and laying the foundation for future turnover studies in organoids. Our approach has been optimized to produce robust and consistent data from a variety of protein processing and mass spectrometry methods.

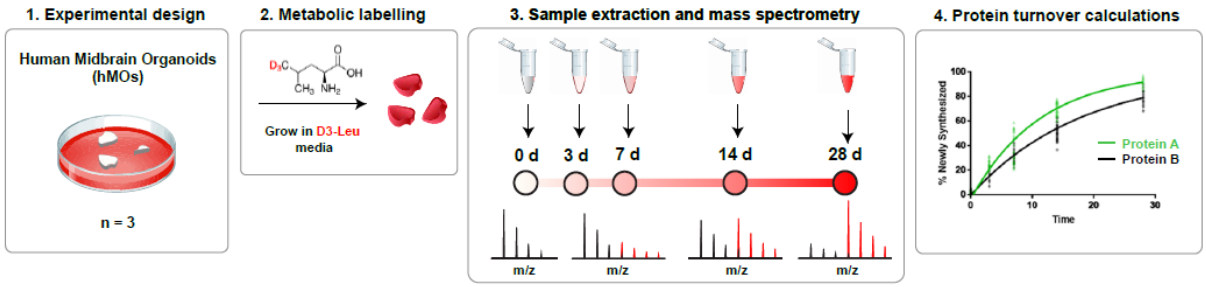

Figure 2.1. Experimental overview. Human midbrain organoids derived from healthy iPSC lines were metabolically labelled with D3-Leu SILAC media over a time course experiment. The organoids were processed at 5 different time points to extract proteins and digest into peptides for MS analysis at each time-point. Protein identifications and the rate of heavy isotope incorporation were determined using MaxQuant, Skyline, and Topograph software.

2.2 Methods

Cell-line information and ethical approvals

The use of iPSCs in this research is approved by the McGill University Health Centre Research Ethics Board (DURCAN_IPSC / 2019-5374). AIW002 lines come from C-BIG repository, The Neuro.

2.2.1 Organoid Generation

Human midbrain organoids (hMOs) derived from healthy individuals were provided by the Neuro's Early Drug Discovery Unit (https://www.mcgill.ca/neuro/open-science/eddu). The complete procedure regarding generation is described in the standardized protocol ref: https://doi.org/10.12688/mniopenres.12816.2 (N. v Mohamed et al., 2021). For Parkin-knockout (PKO) in AIW002-02 iPSCs, gRNAs were designed in exon 2 and cloned into the PX459 vector. After transfection and colonies selection, Sanger sequencing showed

one clone contained a homozygous 77 bp deletion, resulting in a frameshift mutation (C. X.-Q. Chen et al., 2022).

2.2.2 In Vivo Stable Isotope Labeling of hMOs

The SILAC time course experiment consisted of triplicate hMOs (n = 3) at five different time points: Day 0, 3, 7, 14 and 28. Sixty-day old hMOs were incubated in light SILAC media (Table 2). After 7 days of incubation, 3 hMOs were extracted as day 0 (baseline), flash frozen and stored at -80°C until needed. The remaining hMOs were transferred to heavy SILAC media and left to incubate for the corresponding number of days. Both heavy and light media were changed every 2-3 days. All other hMOs were then extracted, frozen, and stored at each designated timepoint following the time course schedule.

2.2.3 hMOs Sample Preparation

hMOs were removed from -80°C storage and rinsed in buffer (50 mM Tris • HCl, pH 7.5). They were then placed in a Potter-Elvehjem PTFE glass tube Dounce homogenizer with 200 µL of lysis buffer (50 mM Tris • HCl, pH 7.5, 8 M urea, 1 mM EDTA, 1X Halt™ Protease Inhibitor Cocktail, 1X PhosStop™ Phosphatase Inhibitor Cocktail). Detergents may be added in the lysis buffer to improve solubilization of membrane proteins if the downstream steps include in-gel digestion or another detergent removal method. Each hMO was homogenized in the lysis buffer with 30-35 pestle strokes and transferred to a 1.5 mL Eppendorf. The tubes were sonicated in a bath sonicator for 10 minutes and spun at 16,000 g for 10 minutes at 4°C. The supernatants were collected and placed into new low-bind 1.5 mL tubes on ice. Protein concentrations of each supernatant were measured

using Pierce BCA protein assay kit, according to manufacturer's instructions. All samples were normalized to 1 µg /µL in 1X Laemmli buffer and were boiled at 80°C for 5 minutes for subsequent SDS-PAGE in-gel digestion.

2.2.4 In-Gel Digestion

For each sample, 20 µg of organoid lysates were loaded onto a 10% Mini-PROTEAN® TGX™ Precast Protein Gels (50 µl wells). Samples were run at 100 V until the samples migrated fully into the stacking region of the gel. Protein bands were visualized using SimplyBlue™ SafeStain (ThermoFisher), according to manufacturer instructions. Each sample was excised in a single band using a clean razor blade, and in-gel digestion was performed as previously described (Shevchenko et al., 2006). Briefly, each band was destained, reduced with 10 mM DTT, alkylated with 55 mM iodoacetic acid, and digested with trypsin overnight at 37 °C. Digested peptides were extracted with 1:2 (vol/vol) 5% formic acid / acetonitrile, transferred to a clean 1.5 mL Eppendorf tube, and dried in a Savant SPD2010 SpeedVac (ThermoFisher). Peptides were re-suspended in 0.1 % formic acid. At this stage, peptides can either be loaded by equal volumes or can be normalized using the Pierce Quantitative Colorimetric Peptide assay, according to manufacturer's instructions.

2.2.5 LC-MS/MS

2 µg of extracted peptides were re-solubilized in 0.1% aqueous formic acid / 2% acetonitrile and loaded onto a Thermo Acclaim Pepmap (Thermo, 75 µm ID X 2 cm C18 3 µm beads) pre-column and then onto an Acclaim Pepmap EASY-Spray (Thermo, 75

μm X 15 cm with 2 μm C18 beads) analytical column separation using a Dionex Ultimate 3000 uHPLC at 250 nl/min with a gradient of 2-35% organic (0.1% formic acid in acetonitrile) over 3 hours. Peptides were analyzed using a Thermo Orbitrap Fusion mass spectrometer operating at 120,000 resolution (FWHM in MS1) with HCD sequencing (15,000 resolution) at top speed for all peptides with a charge of 2+ or greater.

2.2.6 Data Processing

Our data processing protocol is easily portable to data generated from different mass spectrometer vendors and/or digestion methods, as it utilizes freely available, open-source software. The basic workflow consists of: (1) peptide identification from raw data files in MaxQuant; (2) spectral library building in Skyline; (3) protein half-life determination in Topograph; (4) data parsing, filtering, and analysis.

2.2.6.1 Peptide Identification and Database Search with MaxQuant

RAW mass spectra data was processed using Andromeda, integrated into MaxQuant (version 1.6.10) (Cox & Mann, 2008). While MaxQuant has the ability to specify heavy labels and calculate H:L peptide ratios directly, our workflow uses MaxQuant solely as a means for protein identification for spectral library building in Skyline.

1. In “Configuration”, select ‘Add’ to introduce a custom modification that has not been defined in MaxQuant. For this example, D3-Leucine “H(-3) 2H(3)”, with a mass change of 3.0188u were inputted as a standard type modification. Press the “Modify Table” to transfer the custom modification to the modification list in MaxQuant. Click “Save Changes”, and restart MaxQuant.

2. Load all RAW data into MaxQuant using “Load folder” with “Recursive” selected, and give each file a name with “Set experiment”. Biological replicates must have unique experiment names (eg. run_1, run_2, run_3), as they will be combined later in Topograph.
3. In “Group-specific parameters”, select carbamidomethylation (C) as a fixed modification. Select oxidation (M), protein acetylation (N-term), and D3-Leucine as variable modifications. For instrument parameters, select default MaxQuant parameters for an Orbitrap, including a first search peptide tolerance of 20 ppm and a main search peptide tolerance of 4.5 ppm.
4. Select Trypsin/P as an enzyme for cleavage, and permit a maximum of two missed cleavages.
5. In “Global parameters”, add your FASTA file of interest (ie. reviewed human proteome from UniProt; UP000005640). Select the row and set the identifier rule to “Uniprot identifier”. The minimum peptide length can be left at 7 a.a.
6. In “Identification”, ensure that you select “Match between runs” to enable transferring of protein identifications across runs. All other settings can be left default.
7. Set the number of dedicated processors in the bottom left and start the run.

2.2.6.2 Building Spectral Library through Skyline

Skyline (daily version 21.2.1.403) is an open-source application for targeted proteomics and quantitative data analysis (MacLean et al., 2010). Skyline builds spectral libraries via BiblioSpec from a variety of upstream database searches, including MaxQuant. For additional details and tutorials, visit the Skyline website:

https://skyline.ms/project/home/software/Skyline/begin.view

1. Save RAW files and all MaxQuant output files in the same directory.

2. Create a blank Skyline document and save it the same folder with the RAW data and MaxQuant text file outputs. Navigate to the Modifications.xml in the MaxQuant bin folder and copy it to the same folder.
3. Select ‘File’ to import a ‘Peptide Search’. Click ‘Add Files’ and navigate to the msms.txt file and import with default settings. Ensure that Skyline has found all raw spectrum files by checking the “Results files found” table and add any modifications that have not been defined by Skyline.
4. Select “Orbitrap” for precursor mass analyzer and set the resolving power to 120 000 at 400 m/z. Only scans within 5 minutes of MS/MS IDs were included. These parameters should be adjusted according to the instrument used for the timecourse experiment.
5. Select Trypsin/P [KR | -] as an enzyme for cleavage, and permit a maximum of two missed cleavages.
6. Select the same FASTA file used for the MaxQuant search and click “Finish” to create a BiblioSpec spectral library.

2.2.6.3 Protein Half-Life Calculations with Topograph

Topograph processes spectral libraries to calculate protein turnover rates by analyzing the fraction of heavy labels in newly synthesized proteins. The software is able integrate information from all replicates and timepoints to produce one half-life of a given protein. Furthermore, Topograph considers precursor pool enrichment levels, allowing for accurate calculations when the precursor pool is not fully labeled (Hsieh et al., 2012).

1. Create a new workspace in the same directory as the BiblioSpec library and RAW data files.
2. Navigate to ‘Add Search Results’ to select ‘Import BiblioSpec library’

3. Keep the default static modification (C heavier by 57.021461 Da) and specify the heavy label by selecting the preset ‘D3-Leu’ option. Custom isotope labels can also be configured, if necessary.
4. Select and import RAW data files and begin analysis on peptides with default settings. This process can take several days depending on the complexity, quantity and size of the data.
5. After the peptide analysis is complete, select ‘Set Cohort and Time points of Samples’ and assign time points and the cohort of samples based on the experimental design. Specify the number of biological replicates and conditions associated with the experiment.
6. Prior to calculating half-lives, configure the following parameters under ‘View half-lives’: Select the option to calculate % newly synthesized from ‘Distribution of Unlabeled, Partially Labeled and Fully Labeled Peptides’. Set the percent of label at the start of the experiment to 0 and choose the median precursor pool. Set a minimum intensity of 10^5, minimum deconvolution score of 0.95, minimum turnover score of 0.98, and an outlier filter of TwoStdDev for the acceptance criteria. Choose ‘Simple Linear Regression with 95% CI’ for further statistical analysis. The curve should not be forced through the origin as we suggest evaluating whether there is a time delay from the introduction of the label to the appearance of the label in the peptide (see 2.6.6).
7. To calculate half-lives for each protein, select ‘By Protein’, then click ‘Recalculate’. To calculate half-lives for each peptide, deselect both ‘By Protein’ and ‘By Sample’, then click ‘Recalculate’
8. The corresponding table lists all the identified proteins along with their half-lives and confidence intervals. To customize and view more information surrounding the half-life calculation (such as the rate constant, standard deviation, x-intercept of the linear regression), select the ‘Views’ tab in the middle left of the screen and click ‘Edit View’.
9. Click ‘Export’ to output the viewed data table into a csv file named ‘ResultRow’.

10. Select the ‘View’ tab in the top left and navigate towards the options “Results By Cohort” and “Results By Replicate” to output “DisplayRow” and “PerResultReplicate” as csv files. “Results By Cohort” displays the half-life of each protein separated by RAW file. The information can be customized to display, tracer percentage, and area under the curve under the ‘Views’ tab. “PerResultReplicate” is an overview of all the individual peptides found in each RAW file and displays the tracer percentage on the peptide level.

Note: Topograph groups proteins with shared peptides and assigns a single half-life calculation to that group. These non-unique groups will contain multiple concatenated FASTA headers in the “ProteinName” column. Users should analyze half-lives from ambiguous protein groups at their own discretion.

2.2.6.4 Data Parsing and Filtering

Data cleansing is conducted through Excel and manual validation of the half-life curves.

1. Using the ‘ResultRow.csv’ file, remove all proteins that have ‘NA’ or negative values for their half-life or 95% confidence interval.
2. Data points are defined as any peptide contributing to the $t_{1/2}$ calcuation at any replicate and timepoint. Check the ‘Point_Count’ option in the custom ‘Views’ tab to view the total number of all data points for a given half-life calculation.
3. Topograph can exclude timepoints used in protein half-life calculations by deselecting days in the ‘Included Times’ box. To extract the number of data points for a given protein at any specific time point, ‘Included Times’ was reduced to a single day, half-lives were recalculated by clicking ‘Recalculate’, and the resulting list was exported to CSV. This process was repeated for all time points and appended on a protein level. Only proteins with at least 2 data points detected in 3 different time points were included for further analysis.

4. Divide the range of the 95% confidence interval (upper bound minus lower bound) with the half-life of each individual protein to yield a value analogous to the coefficient of variation. Exclude proteins with a “coefficient of variation” ratio of > 0.3.

2.2.6.5 Protein Abundance Calculations

Topograph sums the peak areas of all forms of both the labeled (heavy) and unlabeled (light) peptide as a measure of total abundance. This abundance should be compared across time-points, either on a peptide or a protein level, to ensure that the steady state assumption remains valid.

1. Normalize the abundance values under the ‘Area’ column found in the ‘ResultsbyCohort.csv’ by dividing each individual value for a protein by the sum of all the values in that biological replicate.
2. Calculate the average abundance values for each protein across all the biological replicates at day 0 and 28.
3. For each protein, perform paired sample t-tests with a Benjamini Hochberg correction with a false discovery rate of 5% to compare the mean abundance values between day 0 and 28.
4. Exclude proteins that have significant differences in mean abundance from further turnover analysis.

2.2.6.6 Assessing Time Delays for Heavy Label Incorporation

The x-intercepts of protein half-life curves can be used to assess the time delay from when the heavy media was first introduced to the organoid to heavy label appearance in a peptide. These intercepts may also be used to gain a qualitative sense of the curve fitting in Topograph, depending on the distribution of x-intercepts across a dataset.

1. Calculate the mean and standard deviation of the x-intercept distribution derived from the filtered dataset in 2.2.6.7.
2. Flag proteins that have a x-intercept 2 standard deviations away from the mean. In our dataset, we have excluded these hits from bulk analysis, though they could be manually inspected prior to inclusion, at the user's discretion.
3. If the dataset is centered around t = 0, recalculate protein half-lives by fitting all proteins through the origin (under 'Curve Fitting' select 'Force curve through origin' and 'Recalculate' – see step 6 of 2.2.6.3). If the dataset is not centered around the origin, Topograph is unable to force curves through non-zero x-intercepts, so we recommend leaving the dataset unforced.

2.2.7 Protein Half-Life Calculations and Monte Carlo Simulation

To calculate protein half-lives, we used the following equation derived from Topograph where n = percent of a peptide that is newly synthesized, λ = the rate constant, *t* = the amount of unlabeled peptide at a given time point, and t_0 = the time delay from the introduction of the heavy label to its appearance in a peptide. In our organoid model, t_0 is 0 days as determined by 2.2.6.6 (Hsieh et al., 2012):

$$1 - n = e^{-\lambda(t - t_0)}$$

1-n (100% pre-existing peptide - %newly synthesized peptide) represents the fraction of remaining unlabeled peptide at a given time point. The natural logarithm can then be applied to the degradation of this pre-existing peptide.

$$\ln(1 - n) = -\lambda(t - t_0)$$

The turnover rate (λ) of a protein is equal to the slope of the linear regression on the degradation of all the peptides identified for that given protein. The half-life can then be calculated with the following formula:

$$T_{1/2} = \frac{\ln(2)}{-\lambda}$$

Monte Carlo simulations were conducted in Python to determine the technical reproducibility of our method by subsampling data points and comparing the subsampled $t_{1/2}$ to the Topograph $t_{1/2}$. For a given protein, n = 3 data points were randomly subsampled 100 times from the total pool of data points identified in Topograph. Simple linear regression through the origin was performed to compute a half-life for each randomly selected n = 3 subsample. The 95% confidence interval of each half-life calculation was determined using the standard error of the regression parameter estimates. The average half-life and confidence interval of the 100 iterations was then calculated for n = 3 data points. This process was repeated through incrementing the subsample n by 1 until n equaled the total pool of data points for a given protein identified in Topograph.

2.2.8 Determining Significant Changes in Protein Turnover Across Cell Lines

For each protein, turnover rates were compared by calculating a fold change in half-life between cell lines (PKO $t_{1/2}$ / WT $t_{1/2}$). P-values were computed for each fold change using a previously established method that determines P-values from 95% confidence intervals for a given ratio (Altman & Bland, 2011). The P-values were adjusted for multiple comparisons by using the Benjamini-Hochberg procedure with a false discovery rate of 5%. Proteins turned over significantly faster or slower (Log_2(Fold Change) > -0.5 and <0.5) were plotted as a volcano plot (Goedhart & Luijsterburg, 2020).

2.2.9 Functional Annotation and Gene Ontology

hMO proteins with confident half-lives (n = 773) were uploaded to STRING (version 11.5), a database to predict and visualize protein interaction networks, by Uniprot ID (Szklarczyk et al., 2019). For ambiguously assigned protein groups, the first FASTA header was chosen as the representative protein and Uniprot ID for that group. Proteins were assigned a functional annotation using information from a variety of resources including gene and protein information databases (COMPARTMENTS and KEGG) (Binder et al., 2014; Kanehisa & Goto, 2000). Gene Ontology enrichment was performed using ShinyGO v0.75 (S. X. Ge et al., 2020). 210 outliers (defined as > 1.5 or < 0.66 fold change) from the mouse cortex vs. hMO correlation were input as Uniprot IDs. The 4337 identified proteins from our MS experiments were used as the background gene list. KEGG was chosen as the pathway database for all diagrams.

2.2.10 Statistical Analysis and Figure Generation

Simple linear regression was conducted using ordinary least squares in the statsmodels Python package. The correlation between the percentage newly synthesized peptides of replicate organoids was graphically visualized using the Matplotlib Python library. The remaining statistical comparisons and generation of figures were performed through GraphPad Prism 7.05 (GraphPad Software).

2.3 Results and Discussion

2.3.1 Robustness and Reproducibility

Overall, a total of 4337 proteins derived from 25144 peptides were identified from our MS data. After removing hits that did not meet the acceptance criteria (CV <0.3, 2 data points across 3 time points, and x-intercept < 2SD outlined in sections 2.2.6.4-2.2.6.5), 773 proteins remained for analysis. For PKO organoids, 602 proteins remained after filtering.

To validate the robustness of our method, we aimed to: (1) compare the inter-replicate variability across time points, and (2) assess how the number of data points affects the reliability of protein-level turnover measurements. First, we compared the tracer percentages for each protein across replicates (n = 3) and time points after coefficient of variation (CV) filtering (Figure 2.2). R^2 values ranged from 0.83 – 0.95 between Day 3 and Day 28 for both organoid genotypes, demonstrating adequate reproducibility across replicates and cell lines. Another important observation is that the organoid proteins reliably increased in heavy label incorporation over time, as seen by the shifts in distribution from 0% tracer at Day 0 to nearly 100% tracer at Day 28. For Day 0, the correlations were weaker (R^2 = 0.43 and 0.59), in part due to the limitation of fitting a 2-D plane to points clustered near (0,0,0), where noisy values can drastically alter R^2 calculations. Most of the outliers which deviated significantly from the 2-D correlation plane were successfully pre-filtered by the steps outlined in 2.2.6.4.

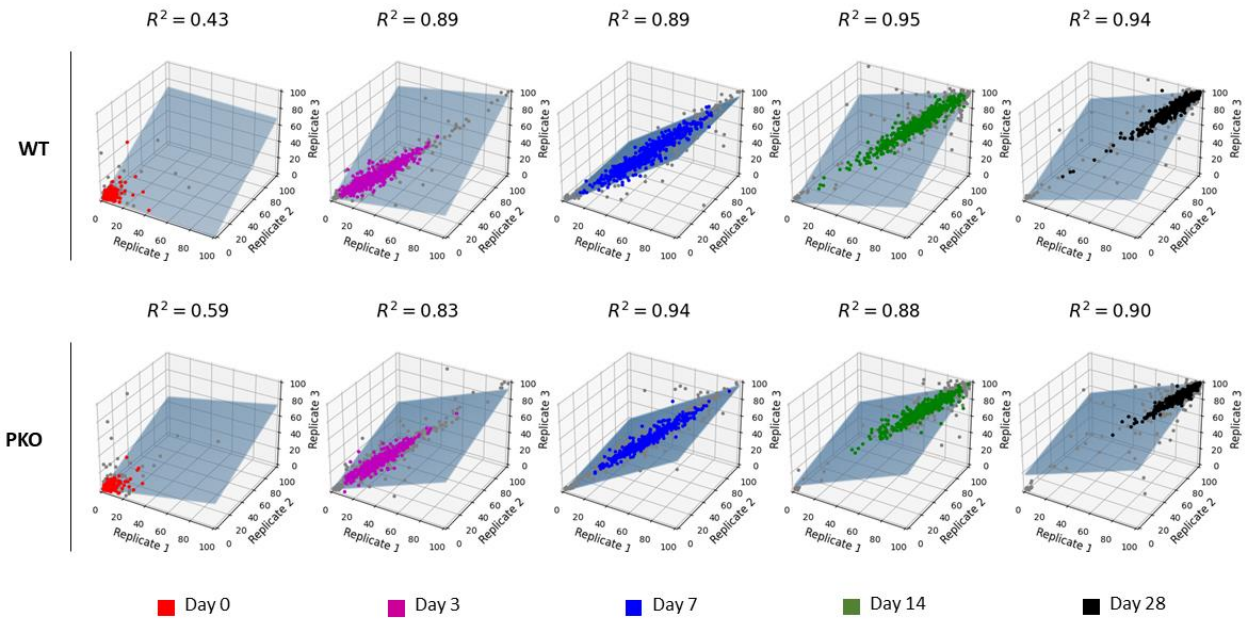

Figure 2.2. D3-Leucine incorporation is strongly correlated across replicates at non-zero time points. The average "% newly synthesized" for all proteins prior to filtering were plotted on a 3-dimensional scatter plot according to time point. Only proteins with 3 valid '% newly synthesized' values at each time point were included. Grey points represent proteins that did not meet the filtering criteria and were excluded from further analysis. The blue plane visualizes the multiple linear regression model of the 3 replicates.

The weaker correlations at Day 0 along with the x-intercept analysis in 2.2.6.5 support the intuitive principle that Day 0 samples are not necessary for confident half-life determinations in SILAC turnover workflows. While it is safe to assume that there will be no heavy labelling at Day 0, we recommend that users investigate the distribution of x-intercepts, which represents the "transit time" of heavy label incorporation in a biological system. In organoids, we demonstrate that there is minimal delay in the initial heavy label uptake, as our global distribution of x-intercepts was centered around 0 days (Supplemental Figure 1A). In mice or other organisms which require absorption via their digestive tract, one would expect longer transit times for the heavy labels and

consequently non-zero, positive x-intercepts in their curve fits. Our dataset also highlighted that Topograph curves whose x-intercepts are extreme outliers (eg. ± 2SD from the total distribution) should be excluded from bulk analysis or analyzed on a case-by-case basis. Datasets which center around a common x-intercept with few extreme outliers may not require this level of filtering stringency.

Next, we evaluated the impact of the number of data points on the quality and accuracy of turnover measurements by performing Monte Carlo subsampling on select proteins and re-calculating each half-life from a subset of data points (Figure 2.3). In Topograph, one “data point” equates to one peptide measured at one time point. In our experimental design (n = 3 replicates across 5 time points), one unique peptide can contribute up to 15 data points for a given half-life calculation. To maximize data completeness, we restricted our analysis onto proteins containing a minimum of 2 data points across 3 time points. This final dataset contained a wide range of data points per protein, ranging from 6 to 501 (median = 27), highlighting the need to unbiasedly visualize how this variation propagates into the final half-life calculation and error estimates. This Monte Carlo based approach can also inform users whether their data point cut-offs for downstream calculations are ideal or how many data points are needed to detect differences between conditions.

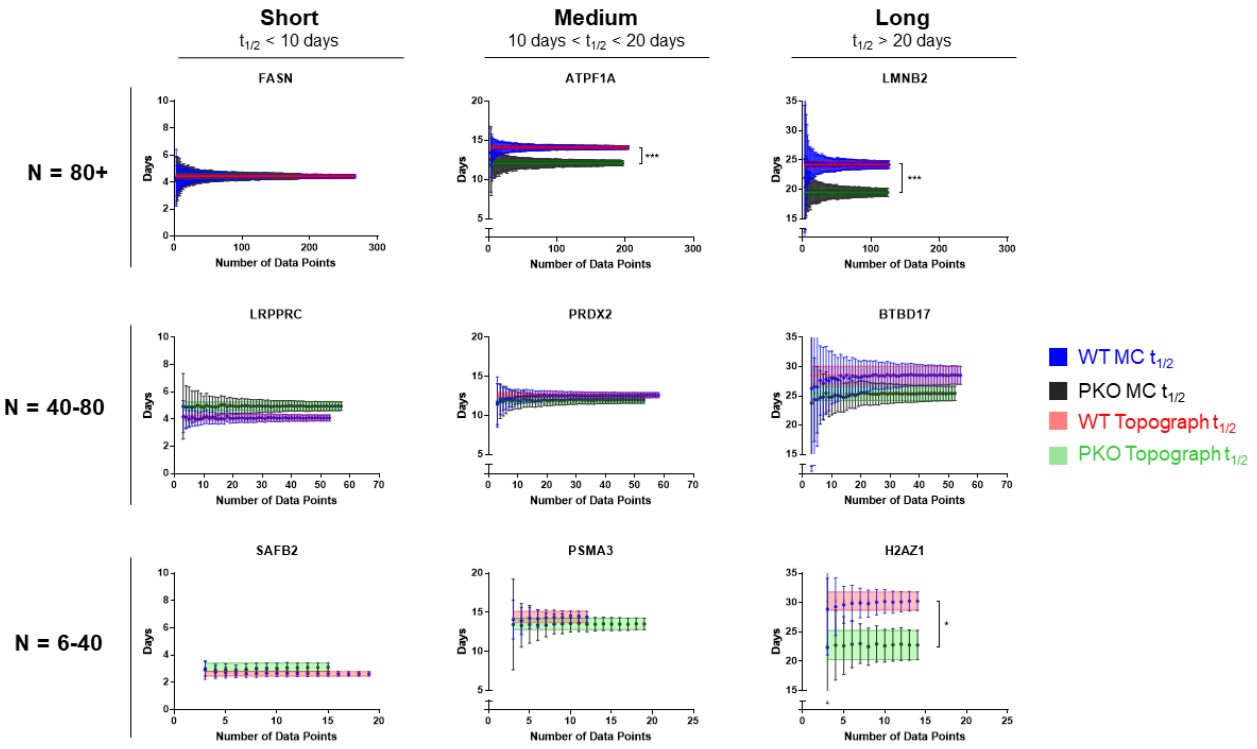

Figure 2.3. Monte Carlo simulations reveal accurate half-lives in subsampled proteins. Blue and black dots represent the average half-life after 100 iterations for each subsample in WT and PKO, respectively. Error bars indicate the average 95% confidence interval of the half-life calculation. Red and green shaded boxes highlight the half-life and 95% confidence interval determined by Topograph using the total pool of identified datapoints.*** $p < 0.0001$ and * = $p < 0.01$ (Benjamini-Hochberg adjusted).

For our dataset, the Monte Carlo simulation demonstrated that the number of data points needed for a confident estimate of $t_{1/2}$ is protein-dependent, but that reliable estimates of $t_{1/2}$ can still be achieved with as few as 6 data points in some cases (eg.SAFB2 in Figure 2.3). For the 9 proteins selected, the average $t_{1/2}$ of 100 Monte Carlo simulations (blue/black dots in Figure 2.3) converged within the 95% confidence interval of the final Topograph $t_{1/2}$ within 3-12 data points. PSA3, whose subsampled errors were large, also had wide 95% confidence intervals in the final half-life calculation from Topograph (see

PKO $t_{1/2}$ in Figure 2.3), suggesting that the final $t_{1/2}$ error estimates are accurate and result in low false positive rates following statistical comparisons.

2.3.2 Characterizing Protein Half-Lives

The successful incorporation of D3-Leu into hMOs following incubation with D3-Leu media can also be visualized by tracking the tracer percentage of specific proteins over time (Figure 2.4A). In the example provided, the electron transport chain protein ATP5F1A yielded a half-life of 14.11 ± 0.23 days in WT hMOs (Figure 2.4B).

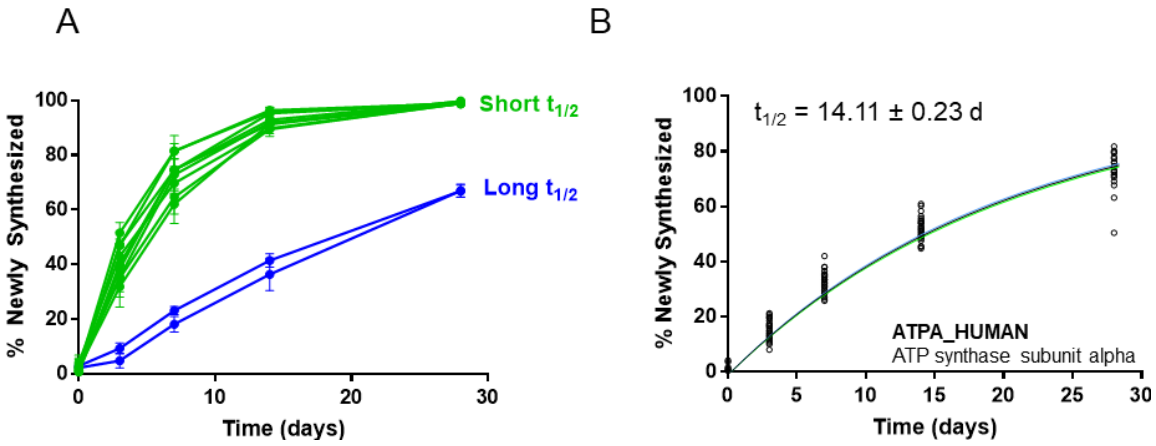

Figure 2.4. D3-Leu incorporates into hMOs and produces robust protein half-life calculations. A) The percentage of newly synthesized peptides for a given protein reliably increases over the time course. Proteins with faster turnover rates highlighted in green reach complete incorporation earlier than proteins with slower turnover rates as depicted in blue. B) Example of Topograph half-life output for ATP synthase subunit alpha. Black circles represent the 23 peptides (204 data points) contributing to the half-life calculation. The blue and green lines indicate the upper and lower bounds of the 95% confidence interval.

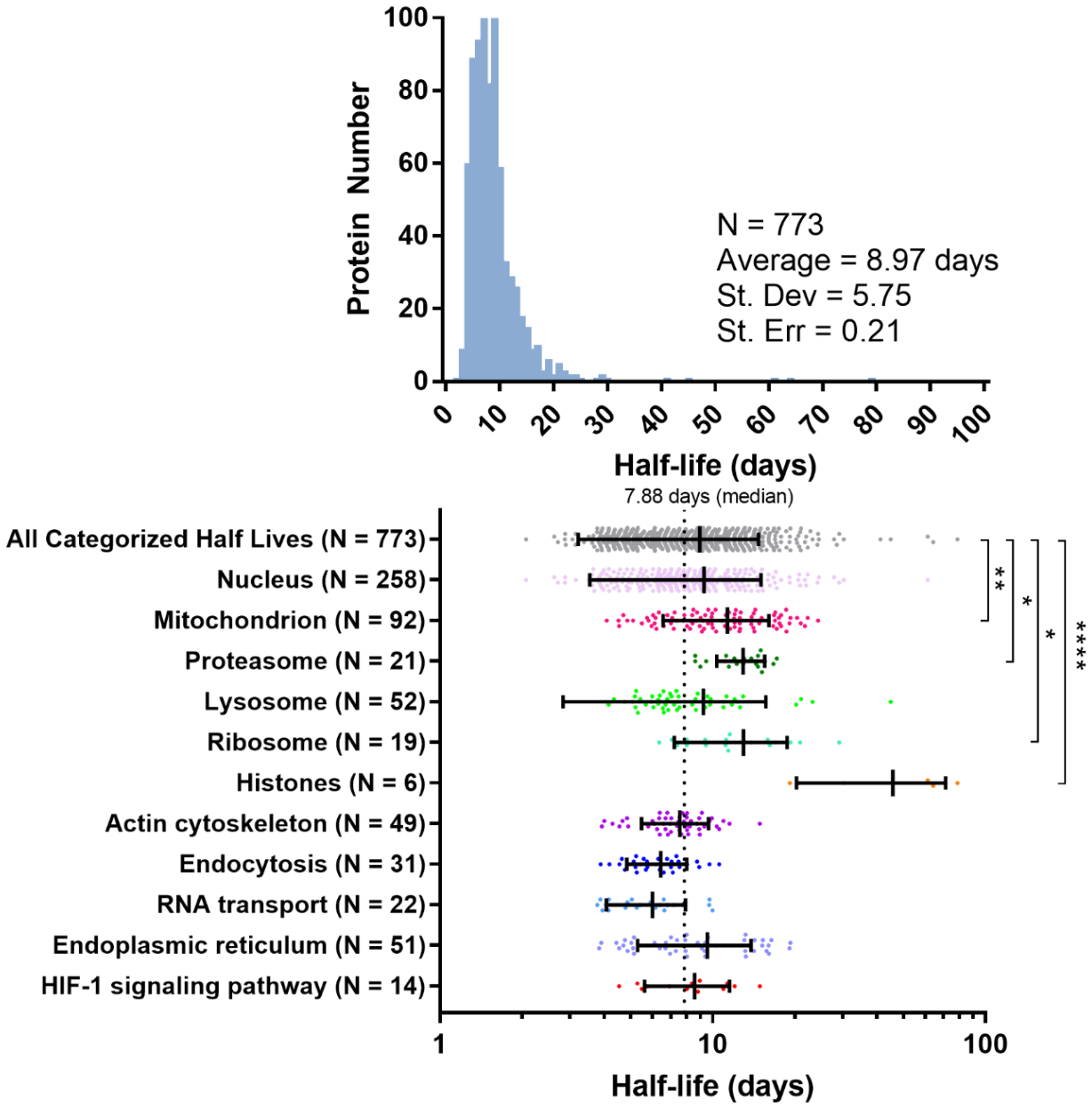

Figure 2.5. Lifetime of midbrain organoid proteins. Lifetimes of proteins organized into groups accordingly to their location and biological pathway. Each data point corresponds to a single protein lifetime. The black lines indicate the mean and the standard deviation (SD) for each group. Analysis of variance (ANOVA) followed by the Dunnett's test summarizes the significance of protein groups compared to the average half-life of all the proteins identified (* ≤ 0.05, ** ≤ 0.01, **** ≤ 0.0001).

Overall, WT hMO half-lives (n = 773) ranged from 2 to 79 days, with a median half-life of 7.9 days. Next, WT hMO half-lives were summarized and grouped according to KEGG annotation and/or cellular localization to investigate trends in compartment- or function-specific turnover rates (Figure 2.5). Most annotations did not deviate significantly from the pool of all characterized half-lives, except for a few notable exceptions: first, mitochondrially localized proteins displayed significantly longer half-lives compared to all measured hMO proteins. Second, histones, proteasomal subunits, and ribosomes were also significantly longer lived. These findings align with previous studies showing the exceptional stability and persistence of histones in mammalian models, most likely to maintain chromatin structure (Fornasiero et al., 2018; Toyama et al., 2013). Proteins associated with RNA transport displayed shorter half-lives, though they did not reach significance when compared to the total pool of hMO proteins. As the emphasis of this work was on method development, we did not focus on the biological implications of these differences, though it is reassuring that these global trends are also seen in other mammalian systems.

In this work, we used PKO organoids as a test case to show that our method is sensitive enough to detect significant differences in protein turnover between organoid genotypes. For the analysis between WT and PKO organoids, we selected the 579 proteins in common between both datasets after CV, data point, and x-intercept filtering. Overall, only ~6% of proteins were significantly different between WT and PKO organoids using a ±1.4 fold change cut-off, highlighting that the majority of protein turnover in organoids is not Parkin-dependent (Figure 2.6). This is not surprising, as basal mitophagy has been

shown to occur independently of Parkin in a variety of organisms and reporter systems (Lee, Sanchez-Martinez, Martinez Zarate, et al., 2018; McWilliams et al., 2018b; Wrighton et al., 2021). Moreover, all the significantly altered proteins exhibited faster turnover in PKO compared to WT hMOs, which suggests that Parkin deletion may have altered the neuronal development or cellular composition of hMOs.

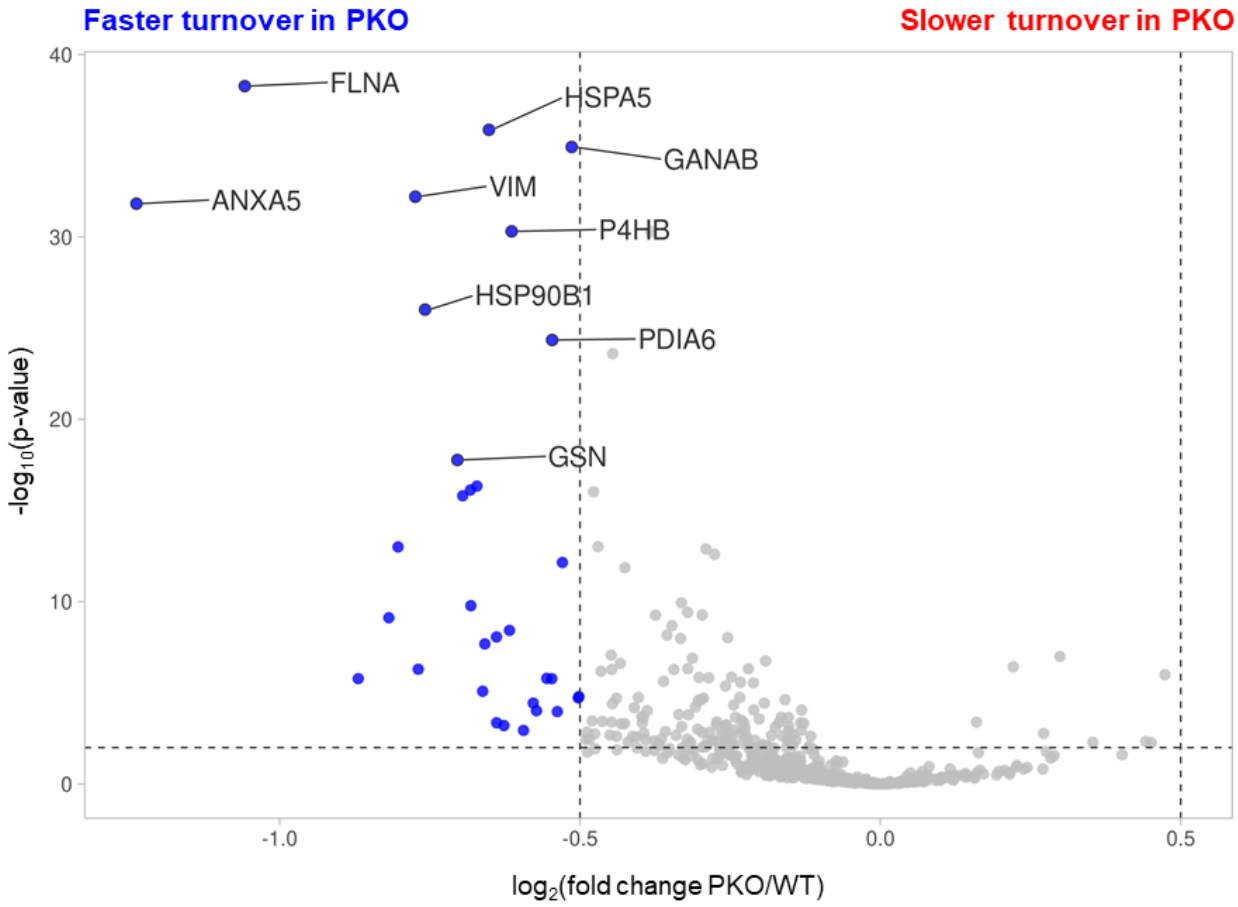

Figure 2.6. Global changes in protein half-lives between WT and PKO organoids. Volcano plot comparing the turnover differences across the 579 proteins that were in common between WT and PKO hMOs after data filtering. Significant hits were defined as those with $p \leq 0.01$ and a $\log_2$ fold change ratio (PKO $t_{1/2}$ / WT $t_{1/2}$) of ≥ 0.5 or ≤ -0.5 (approximately 1.4 fold change)

2.3.3 Comparison of Turnover Rates with Prior Studies

This is the first time that protein half-lives have been characterized in brain organoids. As such, we sought to compare our data with previously published turnover measurements in mice (Fornasiero et al., 2018). When compared to different organs in mice, hMOs were more correlated to mouse cerebellum and cortex than to heart or muscle, albeit modestly (Supplemental Figure 2A). When compared to primary cortical neurons in two separate studies, hMOs were poorly correlated, presumably due to the rapid global turnover of proteins in primary neurons (Supplemental Fig 2B) (Cohen et al., 2013; Heo et al., 2018). To our knowledge, there are no datasets measuring protein turnover in mammalian midbrains, so direct comparisons were not feasible. To investigate whether the lack of correlation between mouse brain regions and hMOs was due to experimental error or a true difference in turnover patterns, we compared a subset of the most confident hits (CV < 0.3) in both datasets (Figure 2.7). The total R^2 did not increase significantly when removing mouse cortex half-lives with higher errors (R^2 = 0.200 in Figure 2.7 vs. R^2 = 0.194 in Supplemental Figure 2A). This lack of increase in correlation suggests that these differences were not due to experimental error. GO analysis on the outliers revealed that human midbrain proteins with different half-lives than mouse cortex were enriched in Parkinson's disease, proteasome, synaptic vesicle cycle, and oxidative phosphorylation GO terms (Figure 2.7). Specifically, respiratory chain proteins were turned over faster in midbrain organoids than in mouse cortex, while proteosomal proteins were turned over slower (Supplemental Data 1).

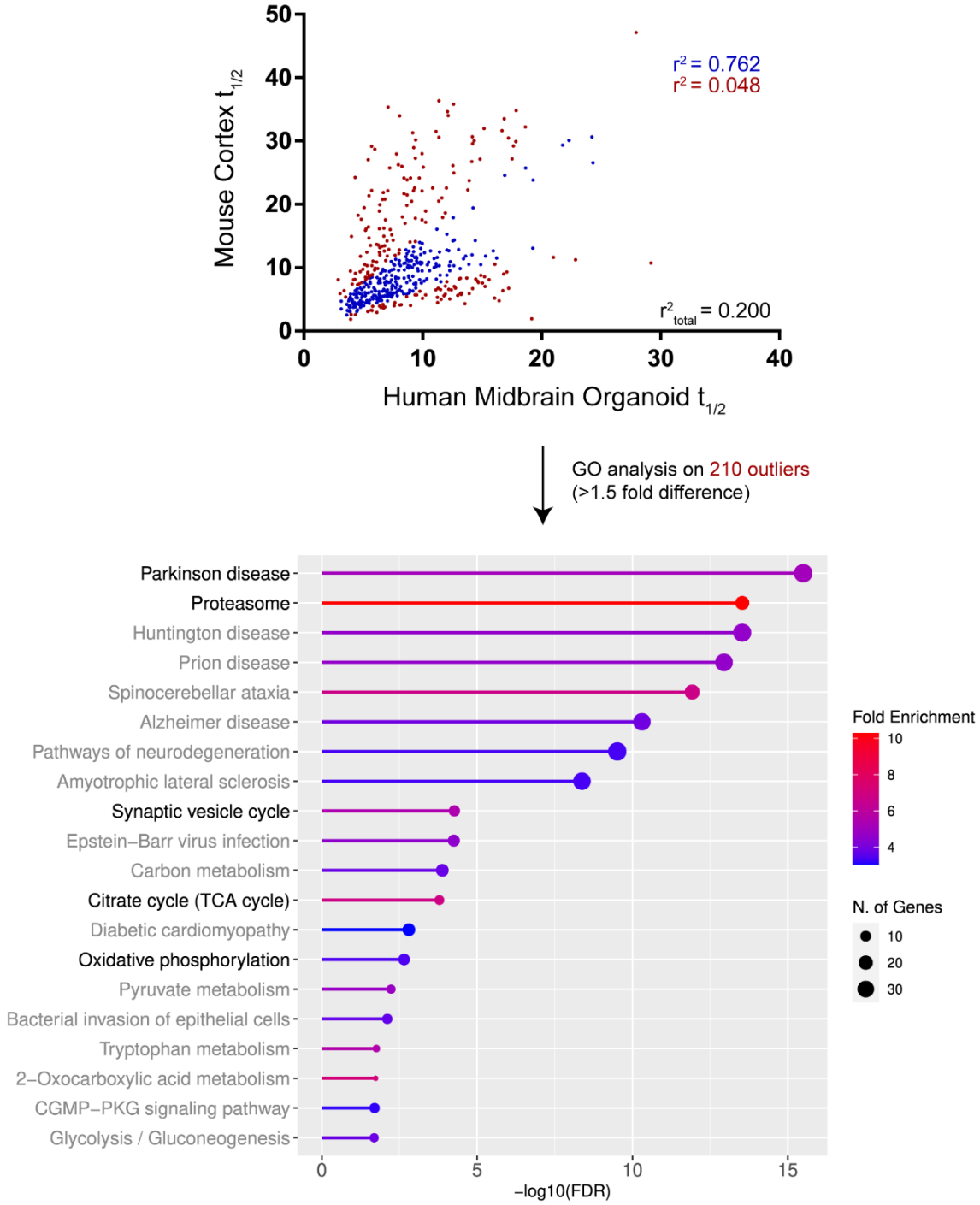

Figure 2.7. Correlation between hMO half-lives and mouse cortex highlights differential protein turnover. Scatterplot comparing the half-lives of hMO proteins (CV < 0.3) to mouse cortex proteins (CV < 0.3). Gene ontology analysis was performed on the correlation outliers (red dots in top panel, defined as fold change >1.5 and < 0.66) in ShinyGO via KEGG. The top 20 most significant hits (FDR corrected p-value < 0.05) were plotted as a lollipop chart and selected GO terms were highlighted in black.

Overall, while both hMO and mouse brain datasets showed that mitochondrial proteins were turned over slower compared to their respective total protein pools, the selective differences highlighted by our GO analysis suggest that midbrains may contain distinct turnover signatures when compared to other parts of the brain. It will be critical to validate whether these differences are truly midbrain specific or whether they represent inherent differences across mammalian model systems.

2.3.4 Limitations

Organoids have immense potential for the modelling and understanding of various diseases, but still suffer from important limitations. Notably, organoids lack an efficient circulatory system leading to issues with oxygen and nutrient exchange (Zhao et al., 2021). Likewise, due to the inherent 3D organization of the tissue culture, nutrient inaccessibility to the inner core can lead to cell necrosis as observed at the core of many reported organoid models (Kelava & Lancaster, 2016). Reduced penetrance of the heavy SILAC label to the organoid center may also contribute to an increased background pool of unlabeled proteins ultimately biasing protein half-life calculations. Recent work has highlighted the utility of microfluidic devices in organoid systems to improve nutrient access and reproducibility in growth, which may also facilitate future studies in hMOs (Velasco et al., 2020). It is also important to note that turnover measurements in their current form necessitate a few key assumptions: (1) the biological system must be in a steady state; this can be verified by quantifying the total level of protein at the beginning and the end of the time course; (2) all fragments of a protein are turned over at the same

rate (i.e. one turnover measurement is calculated for each protein, even if a proteolytic fragment or domain of a protein may be turned over more rapidly). Finally, brain organoids are small and thus axons do not grow more than a few millimeters, whereas axons in mammals can be several centimeters, and even meters. This could create significant differences in the turnover rate of proteins located in the soma compared to the synaptic terminals. In the future, a global comparison of protein turnover results from various turnover software and mathematical models will be useful in order to harmonize and confirm accurate absolute $t_{1/2}$ values across workflows.

2.4 Conclusion

We have provided a robust framework for extracting proteins and measuring global protein turnover in human midbrain organoids. We have also developed a simple analytical and statistical workflow that can be implemented by scientists of all skill levels using open-source or freely available software. Future work using our approach will be able to highlight crucial differences in protein turnover between control and disease models of brain organoids. Overall, our work facilitates the study of proteostasis in organoid models of human disease and will provide a framework to measure protein turnover in organoids of all cell types.

Data Accessibility

The RAW mass spectrometry proteomics data have been deposited to the ProteomeXchange Consortium via the PRIDE (Perez-Riverol et al., 2022) partner

repository with the dataset identifier PXD032169 (username: reviewer_pxd032169@ebi.ac.uk; password: bCJpxdWn).

Supplementary Material

Supplemental Information

Supplemental Data 1

Acknowledgments

We thank the McGill Pharmacology SPR/MS facility (M. Hancock) and the CFI for support, as well as the Proteomics platform at the Research Institute of the McGill University Health Centre (Lorne Taylor, Amy Wong, Jennifer Nedow). This work was supported by an *Innovation Ideas* grant from the *Healthy Brains, Healthy Lives* program at McGill. J.D and A.D were supported by a *Canada Graduate Scholarship* from the Canadian Institutes for Health Research (CIHR), and J.FT. holds a Canada Research Chair (Tier 2) in Structural Pharmacology (CIHR). E.A.F. is supported by a Foundation grant from the CIHR (FDN-154301) and a Canada Research Chair (Tier 1) in Parkinson's Disease.

Table 1: Manufacturer information regarding media and biochemical reagents used for organoid labeling

Reagents	**Supplier / Manufacturer**	**Catalogue Number**
Neurobasal (-L-Leu, -L-Lys, -L-Arg)	Gibco	ME17677L1
L-Leu (Unlabeled)	Cambridge Isotope	ULM-8203-PK
L-Leu (5,5,5-D3 Labeled)	Cambridge Isotope	DLM-1259-1
L-Lys hydrochloride	Thermo Fisher	88429
L-Arg hydrochloride	Thermo Fisher	88427
N2	Gibco	17502048
B27 without vitamin A	Gibco	12587010
GlutaMAX™-I	Gibco	35050-061
Minimum Essential Medium- Non-Essential Amino Acids (MEM-NEAA)	Gibco	11140050
2-mercaptoethanol	Gibco	21985023
Brain-derived Neurotrophic Factor (BDNF)	PeproTech	450-02
Glial cell-derived Neurotrophic Factor (GDNF)	PeproTech	450-10
Ascorbic acid	Millipore Sigma	A5960
Dibutyryl- cyclic AMP (db-cAMP)	Millipore Sigma	D0627
Penicillin-Streptomycin (Penni/Strep)	Millipore Sigma	P0781

Table 2: Recipe for preparation of labeling medium

Reagent and Final Concentration	**Recipe for 50 mL**
Neurobasal (without L-Leu, L-Lys or L-Arg)	50 mL
1:100 N2	0.5 mL
1:50 B27 without vitamin A	1 mL
1% GlutaMAX™-I	0.5 mL
1% MEM-NEAA	0.5 mL
2-mercaptoethanol	0.175 µL
10 ng/mL BDNF	25 µL
10 ng/mL GDNF	25 µL
100 µM ascorbic acid	25 µL
125 µM db-cAMP	12.5 µL
Penni/Strep	0.05 mL
105 mg/L *L-Leu (Unlabeled) / L-Leu (5,5,5-D3 Labeled)	0.5 mL
146 mg/L L-Lys	0.5 mL
84 mg/L L-Arg	0.5 mL

References

Altman, D. G., & Bland, J. M. (2011). How to obtain the P value from a confidence interval. *BMJ*, 343, d2304. https://doi.org/10.1136/bmj.d2304

Andersen, J. S., Lam, Y. W., Leung, A. K. L., Ong, S.-E., Lyon, C. E., Lamond, A. I., & Mann, M. (2005). *Nucleolar proteome dynamics. Nature*, 433(7021), 77–83. https://doi.org/10.1038/nature03207

Bagley, J. A., Reumann, D., Bian, S., Lévi-Strauss, J., & Knoblich, J. A. (2017). Fused cerebral organoids model interactions between brain regions. *Nature Methods*, 14(7), 743–751. https://doi.org/10.1038/nmeth.4304

Binder, J. X., Pletscher-Frankild, S., Tsafou, K., Stolte, C., O'Donoghue, S. I., Schneider, R., & Jensen, L. J. (2014). COMPARTMENTS: unification and visualization of protein subcellular localization evidence. *Database : The Journal of Biological Databases and Curation*, 2014, bau012–bau012. https://doi.org/10.1093/database/bau012

Chen, A., Guo, Z., Fang, L., & Bian, S. (2020). Application of Fused Organoid Models to Study Human Brain Development and Neural Disorders*. Frontiers in Cellular Neuroscience*, 14, 133. https://doi.org/10.3389/fncel.2020.00133

Chen, C. C. W., Erlich, A. T., & Hood, D. A. (2018). Role of Parkin and endurance training on mitochondrial turnover in skeletal muscle. *Skeletal Muscle*, 8(1), 10. https://doi.org/10.1186/s13395-018-0157-y

Chen, C. X.-Q., You, Z., Abdian, N., Sirois, J., Shlaifer, I., Tabatabaei, M., Boivin, M.-N., Gaborieau, L., Karamchandani, J., Beitel, L. K., Fon, E. A., & Durcan, T. M. (2022). Generation of PRKN and PINK1-KO and double KO cell lines from healthy induced pluripotent stem cells using CRISPR/Cas9 editing. *BioRxiv*, 2022.02.25.482014. https://doi.org/10.1101/2022.02.25.482014

Choi, S. H., Kim, Y. H., Hebisch, M., Sliwinski, C., Lee, S., D'Avanzo, C., Chen, H., Hooli, B., Asselin, C., Muffat, J., Klee, J. B., Zhang, C., Wainger, B. J., Peitz, M., Kovacs, D. M., Woolf, C. J., Wagner, S. L., Tanzi, R. E., & Kim, D. Y. (2014). A three-dimensional human neural cell culture model of Alzheimer's disease. *Nature*, 515(7526), 274–278. https://doi.org/10.1038/nature13800

Cohen, L. D., Zuchman, R., Sorokina, O., Müller, A., Dieterich, D. C., Armstrong, J. D., Ziv, T., & Ziv, N. E. (2013). Metabolic turnover of synaptic proteins: kinetics, interdependencies and implications for synaptic maintenance. *PloS One*, 8(5), e63191–e63191. https://doi.org/10.1371/journal.pone.0063191

Cox, J., & Mann, M. (2008). MaxQuant enables high peptide identification rates, individualized p.p.b.-range mass accuracies and proteome-wide protein quantification. *Nature Biotechnology*, 26(12), 1367–1372. https://doi.org/10.1038/nbt.1511

Dakic, V., Minardi Nascimento, J., Costa Sartore, R., Maciel, R. de M., de Araujo, D. B., Ribeiro, S., Martins-de-Souza, D., & Rehen, S. K. (2017). Short term changes in the proteome of human cerebral organoids induced by 5-MeO-DMT. *Scientific Reports*, 7(1), 12863. https://doi.org/10.1038/s41598-017-12779-5

Dennissen, F. J. A., Kholod, N., & van Leeuwen, F. W. (2012). The ubiquitin proteasome system in neurodegenerative diseases: Culprit, accomplice or victim? *Progress in Neurobiology*, 96(2), 190–207. https://doi.org/https://doi.org/10.1016/j.pneurobio.2012.01.003

Duan, Y., Li, F., Li, Y., Tang, Y., Kong, X., Feng, Z., Anthony, T. G., Watford, M., Hou, Y., Wu, G., & Yin, Y. (2016). The role of leucine and its metabolites in protein and energy metabolism. *Amino Acids*, 48(1), 41–51. https://doi.org/10.1007/s00726-015-2067-1

Fatehullah, A., Tan, S. H., & Barker, N. (2016). Organoids as an in vitro model of human development and disease. *Nature Cell Biology*, 18(3), 246–254. https://doi.org/10.1038/ncb3312

Fecto, F., Esengul, Y. T., & Siddique, T. (2014). Protein recycling pathways in neurodegenerative diseases. *Alzheimer's Research & Therapy*, 6(2), 13. https://doi.org/10.1186/alzrt243

Fornasiero, E. F., Mandad, S., Wildhagen, H., Alevra, M., Rammner, B., Keihani, S., Opazo, F., Urban, I., Ischebeck, T., Sakib, M. S., Fard, M. K., Kirli, K., Centeno, T. P., Vidal, R. O., Rahman, R.-U., Benito, E., Fischer, A., Dennerlein, S., Rehling, P., … Rizzoli, S. O. (2018). Precisely measured protein lifetimes in the mouse brain

reveal differences across tissues and subcellular fractions. Nature Communications, 9(1), 4230. https://doi.org/10.1038/s41467-018-06519-0

Goedhart, J., & Luijsterburg, M. S. (2020). VolcaNoseR is a web app for creating, exploring, labeling and sharing volcano plots. Scientific Reports, 10(1), 20560. https://doi.org/10.1038/s41598-020-76603-3

Gonneaud, A., Jones, C., Turgeon, N., Lévesque, D., Asselin, C., Boudreau, F., & Boisvert, F.-M. (2016). A SILAC-Based Method for Quantitative Proteomic Analysis of Intestinal Organoids. Scientific Reports, 6(1), 38195. https://doi.org/10.1038/srep38195

Heo, S., Diering, G. H., Na, C. H., Nirujogi, R. S., Bachman, J. L., Pandey, A., & Huganir, R. L. (2018). Identification of long-lived synaptic proteins by proteomic analysis of synaptosome protein turnover. Proceedings of the National Academy of Sciences of the United States of America, 115(16), E3827–E3836. https://doi.org/10.1073/pnas.1720956115

Hsieh, E. J., Shulman, N. J., Dai, D.-F., Vincow, E. S., Karunadharma, P. P., Pallanck, L., Rabinovitch, P. S., & MacCoss, M. J. (2012). Topograph, a software platform for precursor enrichment corrected global protein turnover measurements. Molecular & Cellular Proteomics : MCP, 11(11), 1468–1474. https://doi.org/10.1074/mcp.O112.017699

Jo, J., Xiao, Y., Sun, A. X., Cukuroglu, E., Tran, H.-D., Göke, J., Tan, Z. Y., Saw, T. Y., Tan, C.-P., Lokman, H., Lee, Y., Kim, D., Ko, H. S., Kim, S.-O., Park, J. H., Cho, N.-J., Hyde, T. M., Kleinman, J. E., Shin, J. H., … Ng, H.-H. (2016). Midbrain-like Organoids from Human Pluripotent Stem Cells Contain Functional Dopaminergic and Neuromelanin-Producing Neurons. Cell Stem Cell, 19(2), 248–257. https://doi.org/10.1016/j.stem.2016.07.005

Kanehisa, M., & Goto, S. (2000). KEGG: Kyoto Encyclopedia of Genes and Genomes. Nucleic Acids Research, 28(1), 27–30. https://doi.org/10.1093/nar/28.1.27

Karbowski, M., & Neutzner, A. (2012). Neurodegeneration as a consequence of failed mitochondrial maintenance. Acta Neuropathologica, 123(2), 157–171. https://doi.org/10.1007/s00401-011-0921-0

Kelava, I., & Lancaster, M. A. (2016). Stem Cell Models of Human Brain Development. *Cell Stem Cell*, 18(6), 736–748. https://doi.org/10.1016/j.stem.2016.05.022

Krüger, M., Moser, M., Ussar, S., Thievessen, I., Luber, C. A., Forner, F., Schmidt, S., Zanivan, S., Fässler, R., & Mann, M. (2008). SILAC Mouse for Quantitative Proteomics Uncovers Kindlin-3 as an Essential Factor for Red Blood Cell Function. *Cell*, 134(2), 353–364. https://doi.org/10.1016/j.cell.2008.05.033

Lee, J. J., Sanchez-Martinez, A., Martinez Zarate, A., Benincá, C., Mayor, U., Clague, M. J., & Whitworth, A. J. (2018). Basal mitophagy is widespread in Drosophila but minimally affected by loss of Pink1 or parkin. *The Journal of Cell Biology*, 217(5), 1613–1622. https://doi.org/10.1083/jcb.201801044

Looso, M., Borchardt, T., Krüger, M., & Braun, T. (2010). Advanced identification of proteins in uncharacterized proteomes by pulsed in vivo stable isotope labeling-based mass spectrometry. *Molecular & Cellular Proteomics : MCP*, 9(6), 1157–1166. https://doi.org/10.1074/mcp.M900426-MCP200

MacLean, B., Tomazela, D. M., Shulman, N., Chambers, M., Finney, G. L., Frewen, B., Kern, R., Tabb, D. L., Liebler, D. C., & MacCoss, M. J. (2010). Skyline: an open source document editor for creating and analyzing targeted proteomics experiments. *Bioinformatics* (Oxford, England), 26(7), 966–968. https://doi.org/10.1093/bioinformatics/btq054

McWilliams, T. G., Prescott, A. R., Montava-Garriga, L., Ball, G., Singh, F., Barini, E., Muqit, M. M. K., Brooks, S. P., & Ganley, I. G. (2018). Basal Mitophagy Occurs Independently of PINK1 in Mouse Tissues of High Metabolic Demand. *Cell Metabolism,* 27(2), 439-449.e5. https://doi.org/10.1016/j.cmet.2017.12.008

Mohamed, N.-V., Lépine, P., Lacalle-Aurioles, M., Sirois, J., Mathur, M., Reintsch, W., Beitel, L. K., Fon, E. A., & Durcan, T. M. (2021). Microfabricated disk technology: Rapid scale up in midbrain organoid generation. *Methods*. https://doi.org/10.1016/J.YMETH.2021.07.008

Mohamed, N.-V., Sirois, J., Ramamurthy, J., Mathur, M., Lépine, P., Deneault, E., Maussion, G., Nicouleau, M., Chen, C. X.-Q., Abdian, N., Soubannier, V., Cai, E., Nami, H., Thomas, R. A., Wen, D., Tabatabaei, M., Beitel, L. K., Singh Dolt, K., Karamchandani, J., … Durcan, T. M. (2021). Midbrain organoids with an SNCA

gene triplication model key features of synucleinopathy. *Brain Communications*. https://doi.org/10.1093/braincomms/fcab223

Mohamed, N. v, Mathur, M., da Silva, R. v, Thomas, R. A., Lepine, P., Beitel, L. K., Fon, E. A., & Durcan, T. M. (2021). Generation of human midbrain organoids from induced pluripotent stem cells [version 2; peer review: 3 approved, 1 approved with reservations] . *MNI Open Research*, 3(1). https://doi.org/10.12688/mniopenres.12816.2

Narendra, D. P., & Youle, R. J. (2011). Targeting mitochondrial dysfunction: role for PINK1 and Parkin in mitochondrial quality control. *Antioxidants & Redox Signaling*, 14(10), 1929–1938. https://doi.org/10.1089/ars.2010.3799

Notaras, M., Lodhi, A., Barrio-Alonso, E., Foord, C., Rodrick, T., Jones, D., Fang, H., Greening, D., & Colak, D. (2021). Neurodevelopmental signatures of narcotic and neuropsychiatric risk factors in 3D human-derived forebrain organoids. *Molecular Psychiatry*. https://doi.org/10.1038/s41380-021-01189-9

Ong, S.-E., Kratchmarova, I., & Mann, M. (2003). Properties of 13C-Substituted Arginine in Stable Isotope Labeling by Amino Acids in Cell Culture (SILAC). *Journal of Proteome Research*, 2(2), 173–181. https://doi.org/10.1021/pr0255708

Ong, S.-E., & Mann, M. (2005). Mass spectrometry–based proteomics turns quantitative. *Nature Chemical Biology*, 1(5), 252–262. https://doi.org/10.1038/nchembio736

Perez-Riverol, Y., Bai, J., Bandla, C., García-Seisdedos, D., Hewapathirana, S., Kamatchinathan, S., Kundu, D. J., Prakash, A., Frericks-Zipper, A., Eisenacher, M., Walzer, M., Wang, S., Brazma, A., & Vizcaíno, J. A. (2022). The PRIDE database resources in 2022: a hub for mass spectrometry-based proteomics evidences. *Nucleic Acids Research*, 50(D1), D543–D552. https://doi.org/10.1093/nar/gkab1038

Shevchenko, A., Tomas, H., Havli, J., Olsen, J. v, & Mann, M. (2006). In-gel digestion for mass spectrometric characterization of proteins and proteomes. *Nature Protocols*, 1(6), 2856–2860. https://doi.org/10.1038/nprot.2006.468

Son, J. H., Shim, J. H., Kim, K.-H., Ha, J.-Y., & Han, J. Y. (2012). Neuronal autophagy and neurodegenerative diseases. *Experimental & Molecular Medicine*, 44(2), 89–98. https://doi.org/10.3858/emm.2012.44.2.031

Szklarczyk, D., Gable, A. L., Lyon, D., Junge, A., Wyder, S., Huerta-Cepas, J., Simonovic, M., Doncheva, N. T., Morris, J. H., Bork, P., Jensen, L. J., & Mering, C. von. (2019). STRING v11: protein-protein association networks with increased coverage, supporting functional discovery in genome-wide experimental datasets. *Nucleic Acids Research*, 47(D1), D607–D613. https://doi.org/10.1093/nar/gky1131

Toyama, B. H., Savas, J. N., Park, S. K., Harris, M. S., Ingolia, N. T., Yates III, J. R., & Hetzer, M. W. (2013). Identification of Long-Lived Proteins Reveals Exceptional Stability of Essential Cellular Structures. *Cell*, 154(5), 971–982. https://doi.org/10.1016/j.cell.2013.07.037

Velasco, V., Shariati, S. A., & Esfandyarpour, R. (2020). Microtechnology-based methods for organoid models. *Microsystems & Nanoengineering*, 6(1), 76. https://doi.org/10.1038/s41378-020-00185-3

Vincow, E. S., Merrihew, G., Thomas, R. E., Shulman, N. J., Beyer, R. P., MacCoss, M. J., & Pallanck, L. J. (2013). The PINK1-Parkin pathway promotes both mitophagy and selective respiratory chain turnover in vivo. *Proceedings of the National Academy of Sciences of the United States of America*, 110(16), 6400–6405. https://doi.org/10.1073/pnas.1221132110

Westman-Brinkmalm, A., Abramsson, A., Pannee, J., Gang, C., Gustavsson, M. K., von Otter, M., Blennow, K., Brinkmalm, G., Heumann, H., & Zetterberg, H. (2011). SILAC zebrafish for quantitative analysis of protein turnover and tissue regeneration. *Journal of Proteomics*, 75(2), 425–434. https://doi.org/https://doi.org/10.1016/j.jprot.2011.08.008

Wrighton, P. J., Shwartz, A., Heo, J.-M., Quenzer, E. D., LaBella, K. A., Harper, J. W., & Goessling, W. (2021). Quantitative intravital imaging in zebrafish reveals in vivo dynamics of physiological-stress-induced mitophagy. *Journal of Cell Science*, 134(4), jcs256255. https://doi.org/10.1242/jcs.256255

Zhao, X., Xu, Z., Xiao, L., Shi, T., Xiao, H., Wang, Y., Li, Y., Xue, F., & Zeng, W. (2021). Review on the Vascularization of Organoids and Organoids-on-a-Chip. *Frontiers in Bioengineering and Biotechnology*, 9, 223. https://doi.org/10.3389/fbioe.2021.637048

Supplemental information

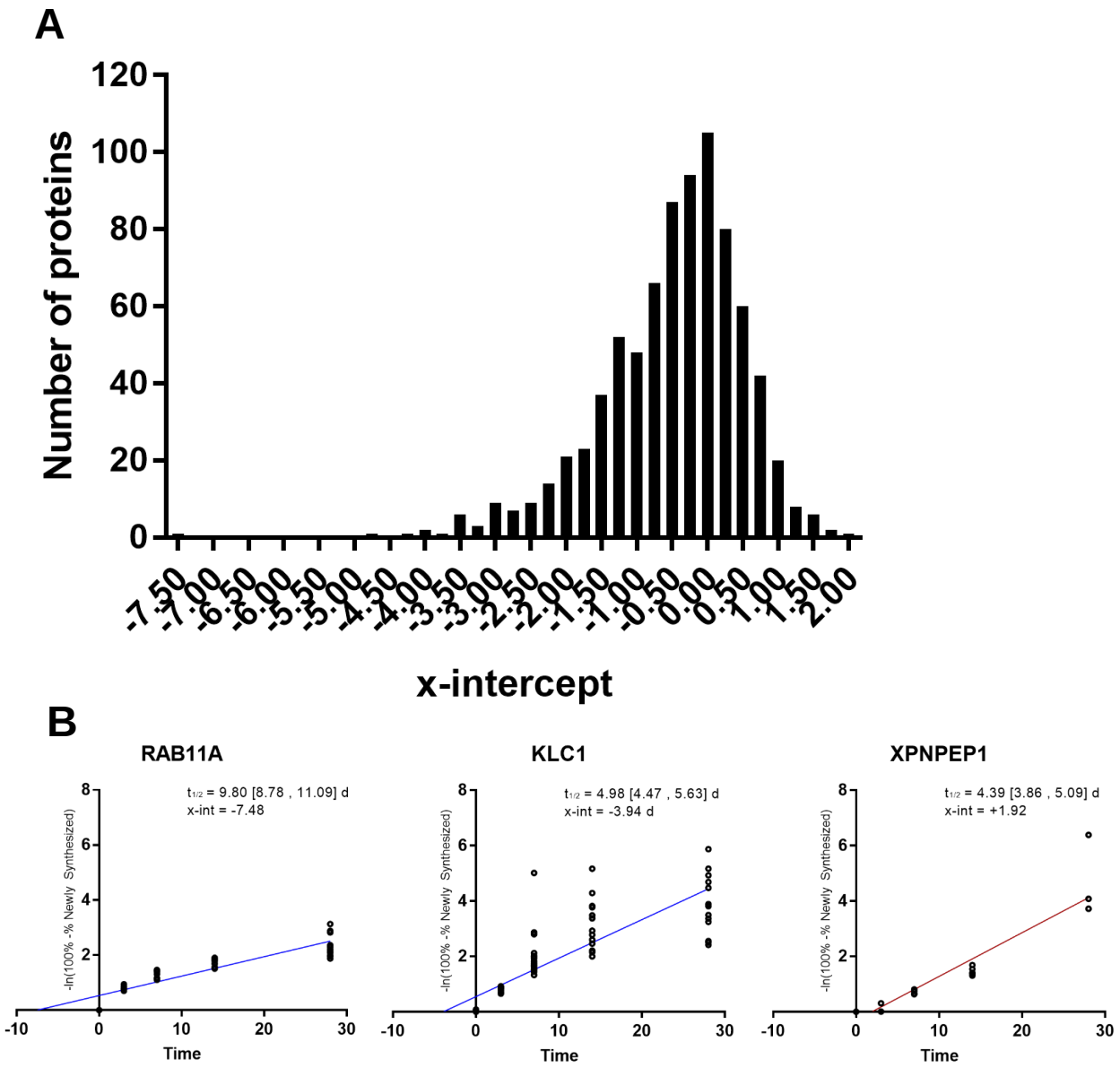

Supplemental Figure 1. Visualization of global x-intercept distribution and outliers prior to 2 SD filtering. A) Frequency histogram of the x-intercepts ("transit times") for all n = 813 characterized proteins prior to 2 SD filtering, which reduced the hits to n = 773. B) Sample curves of proteins with extreme negative (blue) or positive (red) x-intercepts based on Topograph fitting. These proteins were filtered out of the final dataset as they lie 2 SD away from the mean.

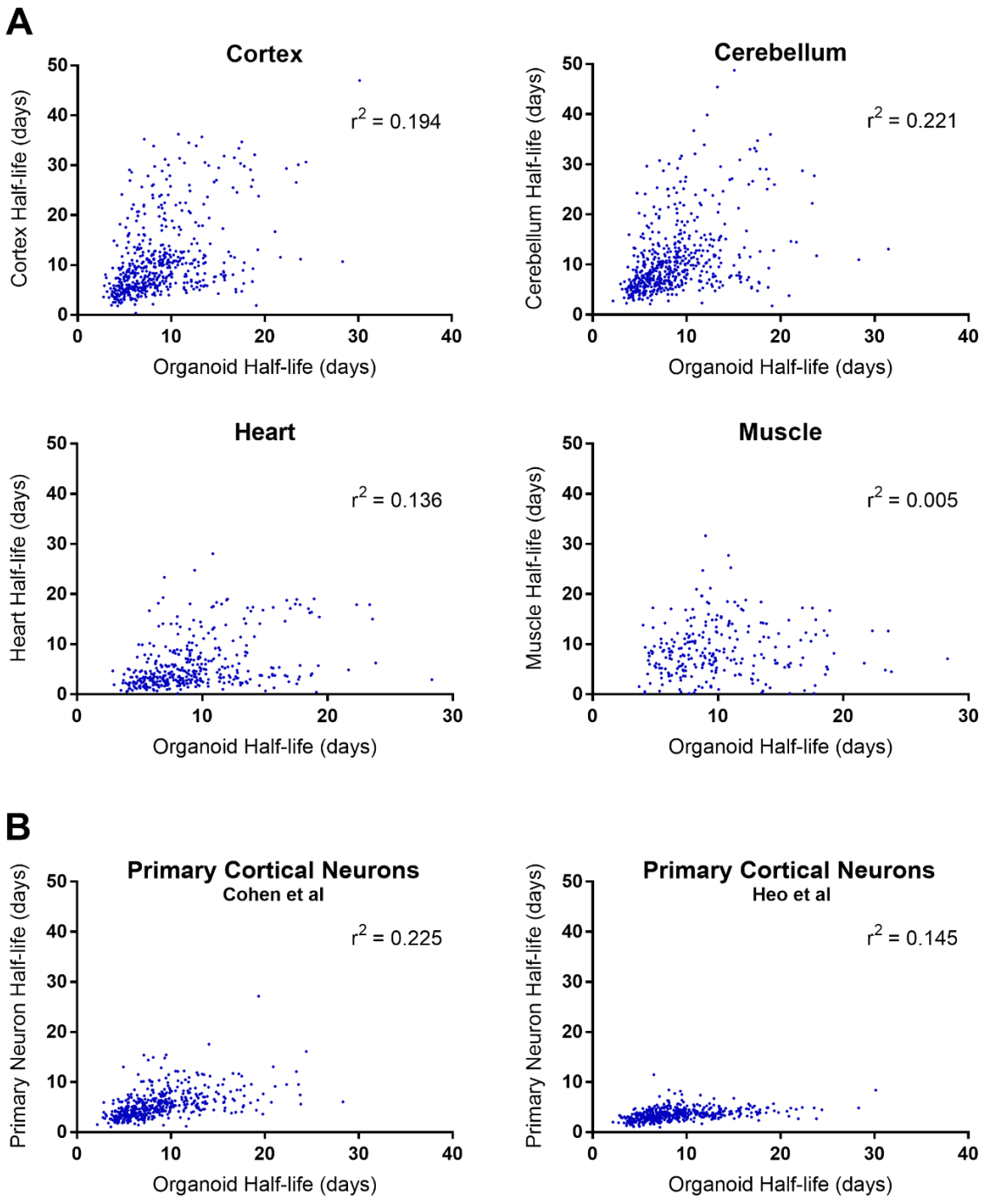

Supplemental Figure 2. Correlation between global hMO half-lives with mice and primary cortical neurons. Scatterplots comparing the half-lives of hMO proteins (CV < 0.3 from this study) to all proteins reported in A) various organs in mice and B) rat cortical neurons [42, 43]. Proteins across datasets were matched according to gene name. Pearson's correlation coefficients are denoted by r^2. For comparison of hMO $t_{1/2}$ CV < 0.3 to mouse cortex $t_{1/2}$ CV < 0.3, see Figure 2.7.

Chapter 3 Discussion

3.1 Methodological Contributions

The present work highlights a new standardized workflow that can be applied to measure proteome-wide turnover. The significance of our methodology is its flexibility, as it is not restricted to PD, but can be extended to other diseases and model systems. Specifically, there are three key methodological contributions in regards to data analysis.

First, we established a software pipeline for analyzing turnover data comprised of *MaxQuant* for peptide identification, spectral library construction with *Skyline*, and protein half-life calculation using *Topograph*. This pipeline is applicable to proteomics data extracted from various different sources. Furthermore, we identified the optimal search parameters and offered user-friendly instructions on how to navigate the program settings of each software as documentation was limited. Second, we created a robust sequence of processing steps that yield high quality protein half-lives composed of filtering on the CV, time delay of tracer incorporation, point count, and protein abundance. The novelty is that we validated our protein half-lives using a Monte-Carlo simulation to prove the robustness of the calculations. To the best of our knowledge, this technique has not yet appeared in filtering steps from other protein turnover studies. It ensures that only the most robust data points make it to the final data set. Third, we demonstrate that our method is able to detect statistical differences in turnover rates across separate genotypes. This establishes the foundation for future research that aims to investigate different pathways and genes of interest involved in proteostasis.

However, challenges still remain which restrict the methods applicability and ability to identify significant trends. Although our results characterized the half-lives of 773 proteins, this barely scratches the surface of the entire human proteome, which is approximately 20,000 (Kim et al., 2014). Another constraint is that we are unable to identify the cellular origin of a given identified protein. Some of our protein hits were associated with astrocytes and bulk sample analysis may fall short of accounting for the heterogeneity of each SILAC sample. Advancements in single-cell proteomics allow researchers to sort individual cells and perform turnover analysis on a subset of cells to decode how specific cell-types are impacted and regulated in the nervous system (Kelly, 2020). This increased analytical insight would allow us to identify any microenvironmental factors that influence PQC or shed light on novel cellular subpopulations that could be influenced in neurodegeneration. Recent techniques also present an exciting opportunity to complement and optimize our current established methodology for obtaining turnover rates at a greater depth. The following section will highlight some future advancements that will improve key aspects to the workflow.

3.1.1 Targeted Approaches with Selection Reaction Monitoring Methods

First, data incompleteness is a major constraint on obtaining protein turnover rates. Half-life calculations are derived from aggregating the H:L ratios of all the peptides of a given protein across multiple timepoints. Hence, the quality and accuracy of the half-life measurement is reliant on the ability of the MS instrument to reproducibly and repeatedly identify the same peptides in different samples. This was not the case for the results in Chapter 2 as some proteins were missing peptides across time points and replicates.

Data incompleteness was incorporated in our stringent filtering process and thus resulted in the removal of many protein hits. This can be attributed to the consequences of operating our MS instrument in Data Dependent Acquisition (DDA) mode for discovery proteomics. DDA selects ions to fragment by high-energy collision dissociation (HCD) based on the most intense ions observed in the MS1 scans (Davies et al., 2021). However, due to fluctuations in scan times or minor differences in liquid chromatography, peptides selected for fragmentation can vary from run to run (H. Liu et al., 2004). Different peptide fragmentations can result in their misidentification which omits them from the aggregate protein half-life calculations. Hence, the nature of DDA contains inherent variation when sampling peptides which contribute to incomplete data acquisition for protein turnover studies (Tabb et al., 2010). Selection Reaction Monitoring (SRM) is a targeted MS/MS technique that can address this issue through boosting sensitivity and selectivity. Principally, SRM employs triple quadrupole MS instruments enabling the user to specify *m/z* filters to select certain peptides for fragmentation (Picotti & Aebersold, 2012). As opposed to scanning over a large mass to charge range, a peptide *m/z* can be specified to achieve maximal sensitivity. The complexity of the proteome is often difficult to resolve but SRM proteomics allows for high sequence-based selectivity (Vidova & Spacil, 2017). Since only a window of *m/z* are transmitted to the MS detector, a predetermined list of target peptides belonging to specific proteins can be selectively investigated. This allows SRM to uniquely target precise biological functions and pathways, or validate significant protein hits in turnover studies. Indeed, a number of SRM based proteomic approach have been used to uncover important protein dynamics (Bisson et al., 2011; Konvalinka et al., 2013). Similarly, a combination of SRM-SILAC

methodology can be used to interrogate protein turnover. Performing SRM techniques on a subset of proteins involved in a pathway of interest will allow us to increase the accuracy and number of peptides identified to generate a more holistic protein half-life. For example, an SRM adapted approach in Chapter 2 could investigate a list of subunits in the respiratory chain to drive a more powerful discovery regarding Parkin's impact on oxidative phosphorylation. Through specifying particular isolation windows, we can increase our visibility and identification of certain peptides across all time points and replicates.

3.1.2 Isobaric Tagging combined with SILAC approaches

Another practical constraint surrounding the methodology is the cost and scalability of the SILAC time course experiment. For example, an experiment comprised of 5 time points, 3 replicates, and 2 genotypes translates to 30 total samples that require individual LC-MS/MS runs (5 x 3 x 2). It is clear that any addition of new genotypes or time points of interest can quickly strain the limited time and resources available. Isobaric tagging combined with SILAC hyperplexing is an innovative MS technique that could potentially alleviate this issue (Welle et al., 2016). Briefly, Tandem Mass Tags (TMT) are isobaric labels which contain a mass reporter and mass normalizer consisting of different stable isotope configurations. Since, the tags have the same nominal mass, TMT labelled peptides appear at the same *m/z* value in a MS1 scan(Rauniyar & Yates 3rd, 2014). However, the mass reporter can be cleaved off the labelled peptide and be detected by the mass analyzer in the MS2 spectrum (Zhang & Elias, 2017). This strategy allows for

multiple samples to be labelled by distinct TMT isotopic reporter variants and analyzed simultaneously in a single pooled MS run.

Welle et al. demonstrates how this approach can be applied with SILAC to conduct proteome-wide turnover studies. Experimental samples from varying timepoints (ie. Day 0, 3, 7…etc) and separate replicates are labelled with different TMT tags (TMT126, TMT127, TMT128…etc) but pooled together in a single sample. A peptide from the same protein in all the pooled samples will have the same *m/z* in the MS1 spectra. However, it can be designated to the correct replicate and timepoint in the MS2 spectrum due to the distinct mass reporter of each TMT label. Therefore, fragmentation of the SILAC labelled peptide peaks will provide insight regarding the kinetic incorporation and appearance of the heavy label across multiple samples in one LC-MS/MS run.

3.2 Applying protein turnover studies to other PD models

The results in Chapter 2 demonstrate that the majority of the midbrain organoid proteome turnover is Parkin-independent, including most mitochondrial proteins as shown in Table 3.

Table 3: Mitochondrial protein hits

Uniprot	**Gene Name**	**Description**	**WT $t_{1/2}$ (d)**	**PKO $t_{1/2}$ (d)**	**Ratio**	**P**
P34897	SHMT2	Serine hydroxymethyltransferase, mitochondrial	12.17	6.66	0.55	<0.001
P00367	GLUD1	Glutamate dehydrogenase 1, mitochondrial	19.28	11.31	0.59	<0.001
Q13011	ECH1	Delta(3,5)-Delta(2,4)-dienoyl-CoA isomerase, mitochondrial	16.77	11.41	0.68	<0.001
Q9UJZ1	STOML2	Stomatin-like protein 2, mitochondrial	20.37	13.94	0.68	<0.001

O75489	NDUFS3	NADH dehydrogenase [ubiquinone] iron-sulfur protein 3, mitochondrial	9.92	7.14	0.72	<0.001
P49419	ALDH7A1	Alpha-aminoadipic semialdehyde dehydrogenase	12.66	9.29	0.73	<0.001
P30049	ATP5F1D	ATP synthase subunit delta, mitochondrial	18.58	13.71	0.74	<0.001
P49189	ALDH9A1	4-trimethylaminobutyraldehyde dehydrogenase	9.37	6.91	0.74	<0.001
Q8NCW5	NAXE	NAD(P)H-hydrate epimerase	11.19	8.41	0.75	<0.001
P30084	ECHS1	Enoyl-CoA hydratase, mitochondrial	11.97	9.23	0.77	0.005
P23368	ME2	NAD-dependent malic enzyme, mitochondrial	9.93	7.69	0.77	0.002
P36957	DLST	Dihydrolipoyllysine-residue succinyltransferase component of 2-oxoglutarate dehydrogenase complex, mitochondrial	17.82	13.81	0.78	0.003
O43488	AKR7A2	Aflatoxin B1 aldehyde reductase member 2	11.07	8.60	0.78	<0.001
P35232	PHB1	Prohibitin	22.30	17.37	0.78	<0.001
P22695	UQCRC2	Cytochrome b-c1 complex subunit 2, mitochondrial	17.79	13.91	0.78	<0.001
P30048	PRDX3	Thioredoxin-dependent peroxide reductase, mitochondrial	14.79	11.72	0.79	<0.001
P07954	FH	Fumarate hydratase, mitochondrial	16.91	13.43	0.79	<0.001
P48735	IDH2	Isocitrate dehydrogenase [NADP], mitochondrial	11.58	9.21	0.80	<0.001
O95831	AIFM1	Apoptosis-inducing factor 1, mitochondrial	12.53	10.03	0.80	<0.001
P07195	LDHB	L-lactate dehydrogenase B chain	14.88	11.92	0.80	<0.001
P09622	DLD	Dihydrolipoyl dehydrogenase, mitochondrial	15.11	12.31	0.81	0.003
Q99623	PHB2	Prohibitin-2	21.77	17.75	0.82	<0.001
P06576	ATP5F1B	ATP synthase subunit beta, mitochondrial	17.48	14.30	0.82	<0.001
P22234	PAICS	Multifunctional protein ADE2	9.97	8.17	0.82	0.002
Q9HC38	GLOD4	Glyoxalase domain-containing protein 4	8.71	7.18	0.82	0.002
Q13423	NNT	NAD(P) transhydrogenase, mitochondrial	9.64	7.95	0.82	0.016
P08559	PDHA1	Pyruvate dehydrogenase E1 component subunit alpha, somatic form, mitochondrial	9.30	7.73	0.83	0.005
P05141	SLC25A5	ADP/ATP translocase 2	10.17	8.50	0.84	<0.001
P10809	HSPD1	60 kDa heat shock protein, mitochondrial	18.66	15.61	0.84	<0.001
P00441	SOD1	Superoxide dismutase [Cu-Zn]	12.04	10.13	0.84	0.003
P36542	ATP5F1C	ATP synthase subunit gamma, mitochondrial	16.64	14.02	0.84	<0.001
P61604	HSPE1	10 kDa heat shock protein, mitochondrial	13.76	11.65	0.85	<0.001

Q16891	IMMT	MICOS complex subunit MIC60	13.88	11.76	0.85	0.011
P48047	ATP5PO	ATP synthase subunit O, mitochondrial	16.97	14.45	0.85	<0.001
P05141	SLC25A5	ADP/ATP translocase 2	9.34	7.97	0.85	0.120
P25705	ATP5F1A	ATP synthase subunit alpha, mitochondrial	14.11	12.12	0.86	<0.001
P04179	SOD2	Superoxide dismutase [Mn], mitochondrial	17.60	15.36	0.87	0.019
P51659	HSD17B4	Peroxisomal multifunctional enzyme type 2	8.18	7.14	0.87	0.002
P00505	GOT2	Aspartate aminotransferase, mitochondrial	17.16	15.01	0.87	<0.001
Q04837	SSBP1	Single-stranded DNA-binding protein, mitochondrial	21.01	18.44	0.88	0.149
P38646	HSPA9	Stress-70 protein, mitochondrial	6.62	5.81	0.88	0.003
Q9BPW8	NIPSNAP1	Protein NipSnap homolog 1	16.81	14.79	0.88	0.070
P32119	PRDX2	Peroxiredoxin-2	12.88	11.34	0.88	0.019
P21796	VDAC1	Voltage-dependent anion-selective channel protein 1	10.02	8.84	0.88	<0.001
P27695	APEX1	DNA-(apurinic or apyrimidinic site) endonuclease	9.40	8.41	0.89	0.138
Q12931	TRAP1	Heat shock protein 75 kDa, mitochondrial	5.75	5.16	0.90	0.062
P45880	VDAC2	Voltage-dependent anion-selective channel protein 2	9.91	8.92	0.90	<0.001
P49411	TUFM	Elongation factor Tu, mitochondrial	8.24	7.44	0.90	0.037
Q99798	ACO2	Aconitate hydratase, mitochondrial	8.41	7.60	0.90	0.002
Q00325	SLC25A3	Phosphate carrier protein, mitochondrial	10.81	9.77	0.90	0.316
P05141	SLC25A5	ADP/ATP translocase 2	10.30	9.33	0.91	0.305
P31040	SDHA	Succinate dehydrogenase [ubiquinone] flavoprotein subunit, mitochondrial	5.81	5.37	0.92	0.361
P30044	PRDX5	Peroxiredoxin-5, mitochondrial	9.05	8.37	0.92	0.110
P31930	UQCRC1	Cytochrome b-c1 complex subunit 1, mitochondrial	14.14	13.22	0.93	0.494
Q9UBQ7	GRHPR	Glyoxylate reductase/hydroxypyruvate reductase	6.33	5.96	0.94	0.558
P32119	PRDX2	Peroxiredoxin-2	12.61	11.99	0.95	0.158
P17612	PRKACA	cAMP-dependent protein kinase catalytic subunit alpha	8.08	7.69	0.95	0.334
Q99497	PARK7	Parkinson disease protein 7	9.13	8.73	0.96	0.315
P09417	QDPR	Dihydropteridine reductase	7.72	7.45	0.96	0.611
O00429	DNM1L	Dynamin-1-like protein	6.13	6.07	0.99	0.921
O00154	ACOT7	Cytosolic acyl coenzyme A thioester hydrolase	5.96	5.92	0.99	0.878
Q9Y277	VDAC3	Voltage-dependent anion-selective channel protein 3	7.79	7.74	0.99	0.954
O75390	CS	Citrate synthase, mitochondrial	9.24	9.24	1.00	0.995
P49327	FASN	Fatty acid synthase	4.44	4.44	1.00	0.983

P24752	ACAT1	Acetyl-CoA acetyltransferase, mitochondrial	7.21	7.23	1.00	0.964
P80404	ABAT	4-aminobutyrate aminotransferase, mitochondrial	10.23	10.36	1.01	0.890
P41250	GARS1	Glycine--tRNA ligase	5.50	5.82	1.06	0.054
Q16881	TXNRD1	Thioredoxin reductase 1, cytoplasmic	6.76	7.48	1.11	0.264
P42704	LRPPRC	Leucine-rich PPR motif-containing protein, mitochondrial	4.09	4.95	1.21	0.006
O43169	CYB5B	Cytochrome b5 type B	6.94	9.42	1.36	0.002
O75746	SLC25A12	Calcium-binding mitochondrial carrier protein Aralar1	5.97	8.16	1.37	0.002

The significantly altered proteins in PKO were surprisingly degraded faster than their WT counterpart which is inconsistent with the observations obtained from the *Drosophila* study conducted by Vincow et al. Despite this, the biological consequence of these protein turnover rates remains to be investigated in other models of PD. Chapter 2 presented limitations inherent to the organoid model growth and development to explain our turnover measurements. The following section will now delve into other future steps to further scrutinize the PQC mechanisms that underlie PD pathogenesis to potentially complement our initial results.

3.2.1 Interrogating other PD-related genes

Examining protein turnover in other familial models will potentially bring to light hidden pathways and proteins that are dysregulated in PD pathology. Future work should look into investigating mutations in other PD-related genes. A spectrum of pathogenic mutations including 7 missense mutations, genomic duplications, and triplications have been reported in SNCA (Fujioka et al., 2014; Konno et al., 2016). Recently, Nguyen et al. developed human midbrain organoids harboring SNCA gene triplication through using CRISPR/Cas9(N.-V. Mohamed, Sirois, et al., 2021b). Notably, these organoids not only

manifested elevated α-syn levels but also displayed α-syn aggregation, a hallmark of patient brains with synucleinopathies. Indeed, both oligomeric and phosphorylated forms of α-syn increased as organoids matured and correlated with the selective DA neuron loss over time. Aggregated α-syn may also inhibit the proteasome through interacting with a subunit of the proteasome 19S cap or interfering with its catalytic activity (Lindersson et al., 2004; Snyder et al., 2003). Apart from disturbing proteasomal function, α-syn has been hypothesized to confer neurotoxic effects through inducing oxidative stress, decrease neurotransmitter release, and inhibit synaptic vesicle recycling (Nemani et al., 2010; Scott et al., 2010; Stefanis, 2012). Proteome wide turnover studies on this model offers an opportunity to narrow down the specific perturbed pathways and pinpoint the exact mechanisms that cause dysregulation.

Another gene central to lysosomal function is GBA. Mutations in the GBA gene encoding for lysosomal enzyme glucocerebrosidase occurs in approximately 5-15% of PD patients (Smith & Schapira, 2022). Likewise, GBA mutations also cause Gaucher's disease, a lysosomal storage disorder which leads to the accumulation of glucocerebroside in tissues such as the liver, spleen, bone, and bone marrow (Rosenbloom & Weinreb, 2013). Observations demonstrating increased rates of Parkinsonism in relatives of Gaucher's disease patients place the gene as a critical genetic risk factor for PD (Halperin et al., 2006). A study conducted in Ashkenazi Jewish patients with PD revealed that approximately one third of the sample cohort harbored a GBA mutation (Aharon-Peretz et al., 2004). Many hypotheses have risen claiming that reduced glucocerebrosidase activity leads to α-syn accumulation or that heterozygous GBA mutations leave patients

vulnerable to a “second hit” involving either another genetic or environmental risk factor. However, studies have yet to demonstrate the accumulation of glucosylceramide, the substrate of glucocerebrosidase, in PD patients with GBA mutations. The mechanistic association between GBA and PD is still unresolved.

A unifying question overarches the series of the PD-associated genes presented in this manuscript such as SNCA, GBA, LRRK2, DJ-1, PINK1, and Parkin. What are the exact mechanisms underlying these genes and how do their impairment translate to selective neuronal death? Would these deficient organisms display impaired turnover of specific cargo required for neuronal health or do they prevent lysosomal function from removing harmful components that target neurons? Future studies should assess global protein turnover of all PD-related genes to uncover pathways and proteins to help piece together this puzzle.

3.2.2 Investigating PINK1/Parkin pathway *in vivo*

The lack of differences observed in mitophagy at baseline when PINK1/Parkin is compromised *in vivo* has been difficult to reconcile. Notably, PINK1/Parkin knock out mice surprisingly fail to capture any meaningful neurological or behavioural phenotypes of PD (Pickrell & Youle, 2015). One intriguing possibility is that an additional stressor is required to trigger the PINK1/Parkin pathway. Although PINK1/Parkin KO mice present no DA neuronal loss, intestinal infection with gram-negative bacteria in PINK1 null mice yielded motor impairment (Matheoud et al., 2019). Likewise, PKO mice that express POLG, a proofreading-defective version of mitochondrial DNA polymerase, exhibited DA neuronal loss and motor deficiencies (Pickrell et al., 2015). The impaired proofreading activity

conferred by POLG introduces mutations in mtDNA and accumulates mitochondrial stress, yet mice expressing POLG alone do not display PD-related phenotypes (Pickrell et al., 2015; Trifunovic et al., 2004). This finding suggests that loss of PINK1/parkin or mitochondrial stress alone may not lead to neurodegeneration but a combination of these events is required to elicit the phenotype. Similar to inactivating a tumor suppressor gene in cancer biology, loss of PINK1/Parkin's protective MQC function can be represented as a "first hit" in a multi-hit model of PD. This is further exacerbated by a "second hit" of mitochondrial stress derived from either bacterial inflammation or the accumulation of mtDNA mutations. This could potentially explain the increase in incidence rate of sporadic PD after 60 years old, as individuals accumulate "hits" over time through other environmental events (de Lau & Breteler, 2006). Whereas, patients with genetically-associated PD have a decreased tolerance to these "hits" due to inadequate PQC mechanisms thus leading to an earlier age of onset for the disease(Alcalay et al., 2010).

Hence, future work should introduce an additional stressor to measure protein dynamics in a multi-hit model of PD *in vivo*. Figure 3 proposes an experimental procedure that extends the approach used in chapter 2 to study protein turnover in mice subject to a stressor, but could also be applied to organoids treated with stressors.

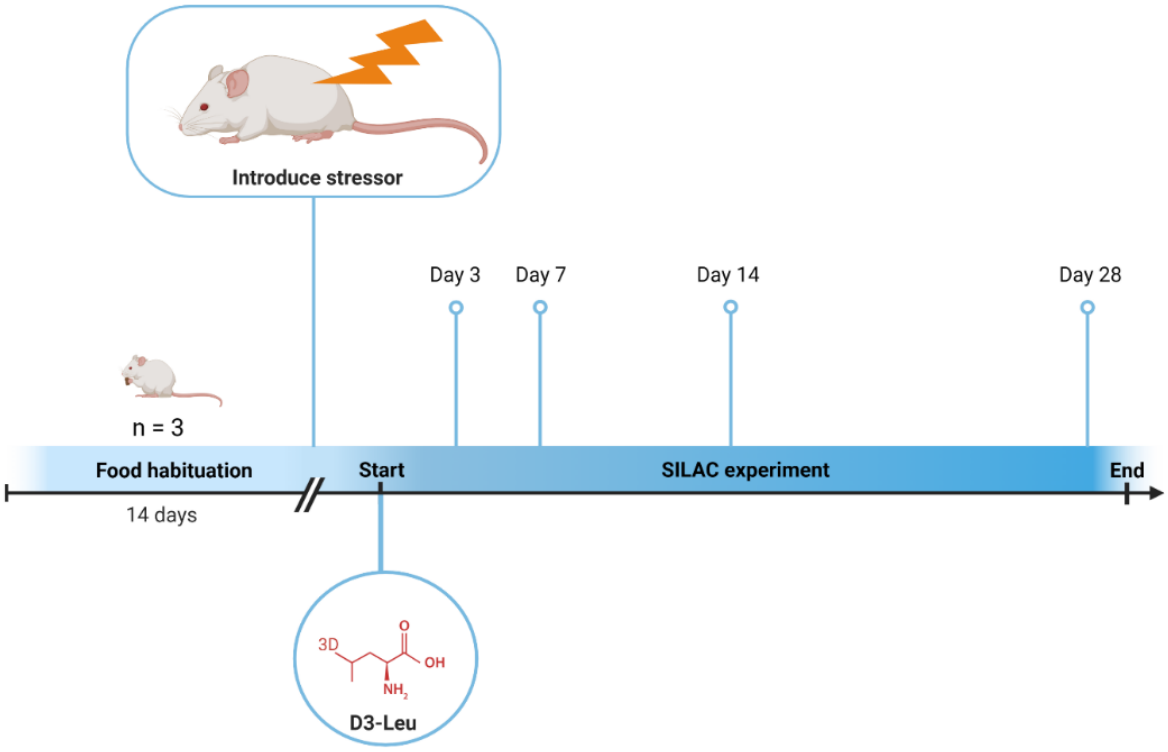

Figure 3: Theoretical experimental overview of *in vivo* turnover measurements.
Briefly, triplicates of PINK1-KO and Parkin-KO mice will be crossed with mutator mice expressing POLG to generate mutant mice in the mutator background. These mice will then be fed a standard unlabelled diet (“light”) for a period of time. After the mice are habituated to their diet, they will switch onto “heavy” labelled food which marks the beginning of the SILAC-time course experiment. A stressor in the form of bacterial infection or exhaustive exercise will be introduced to the mice shortly prior to switching diets to induce inflammation. Proteome wide turnover calculations will be performed to identify dysregulated pathways implicated in neurodegeneration.

3.3 Conclusion

The work contained in this thesis aimed to dissect the mechanisms underlying neurodegeneration through measurement of protein turnover as a proxy for PQC. Regulating protein turnover is an essential component of proteostasis and central to maintaining neuronal health. Thus, we developed a robust workflow and software pipeline to characterize protein half-lives using a SILAC-based quantitative MS approach. We chose to analyze protein turnover in organoids for the first time due to their exciting ability to recapitulate complex features of the brain. A baseline dataset of turnover rates was obtained after a rigorous filtering process and further validated using a multiple probability simulation. The PINK1/Parkin canonical pathway is imperative to MQC and we thus developed a statistical framework to compare global protein turnover with Parkin-*null* organoids. Our work expands our understanding of organoids as a model system and enables powerful research surrounding protein turnover. We hope that the methods and findings presented here will contribute to the discovery of new therapies aimed to improve the lives of patients with PD.

References for Introduction and Discussion (alphabetical)

Aharon-Peretz, J., Rosenbaum, H., & Gershoni-Baruch, R. (2004). Mutations in the glucocerebrosidase gene and Parkinson's disease in Ashkenazi Jews. *N Engl J Med*, *351*(19), 1972–1977. https://doi.org/10.1056/NEJMoa033277

Alcalay, R. N., Caccappolo, E., Mejia-Santana, H., Tang, M. X., Rosado, L., Ross, B. M., Verbitsky, M., Kisselev, S., Louis, E. D., & Comella, C. (2010). Frequency of known mutations in early-onset Parkinson disease: implication for genetic counseling: the consortium on risk for early onset Parkinson disease study. *Archives of Neurology*, *67*(9), 1116–1122.

Altman, D. G., & Bland, J. M. (2011). How to obtain the P value from a confidence interval. *BMJ*, *343*, d2304. https://doi.org/10.1136/bmj.d2304

Andersen, J. S., Lam, Y. W., Leung, A. K. L., Ong, S.-E., Lyon, C. E., Lamond, A. I., & Mann, M. (2005). Nucleolar proteome dynamics. *Nature*, *433*(7021), 77–83. https://doi.org/10.1038/nature03207

Bagley, J. A., Reumann, D., Bian, S., Lévi-Strauss, J., & Knoblich, J. A. (2017). Fused cerebral organoids model interactions between brain regions. *Nature Methods*, *14*(7), 743–751. https://doi.org/10.1038/nmeth.4304

Balch, W. E., Morimoto, R. I., Dillin, A., & Kelly, J. W. (2008). Adapting Proteostasis for Disease Intervention. *Science*, *319*(5865), 916–919. https://doi.org/10.1126/science.1141448

Bayne, A. N., & Trempe, J.-F. (2019). Mechanisms of PINK1, ubiquitin and Parkin interactions in mitochondrial quality control and beyond. *Cellular and Molecular Life Sciences*, *76*(23), 4589–4611. https://doi.org/10.1007/s00018-019-03203-4

Binder, J. X., Pletscher-Frankild, S., Tsafou, K., Stolte, C., O'Donoghue, S. I., Schneider, R., & Jensen, L. J. (2014). COMPARTMENTS: unification and visualization of protein subcellular localization evidence. *Database : The Journal of Biological Databases and Curation*, *2014*, bau012–bau012. https://doi.org/10.1093/database/bau012

Bisson, N., James, D. A., Ivosev, G., Tate, S. A., Bonner, R., Taylor, L., & Pawson, T. (2011). Selected reaction monitoring mass spectrometry reveals the dynamics of signaling through the GRB2 adaptor. *Nature Biotechnology*, *29*(7), 653–658.

Bolam, J. P., & Pissadaki, E. K. (2012). Living on the edge with too many mouths to feed: Why dopamine neurons die. *Movement Disorders*, *27*(12), 1478–1483. https://doi.org/https://doi.org/10.1002/mds.25135

Buscham, T. J., Eichel, M. A., Siems, S. B., & Werner, H. B. (2019). Turning to myelin turnover. *Neural Regen Res*, *14*(12), 2063–2066. https://doi.org/10.4103/1673-5374.262569

Chen, A., Guo, Z., Fang, L., & Bian, S. (2020). Application of Fused Organoid Models to Study Human Brain Development and Neural Disorders. *Frontiers in Cellular Neuroscience*, *14*, 133. https://doi.org/10.3389/fncel.2020.00133

Chen, C. X.-Q., You, Z., Abdian, N., Sirois, J., Shlaifer, I., Tabatabaei, M., Boivin, M.-N., Gaborieau, L., Karamchandani, J., Beitel, L. K., Fon, E. A., & Durcan, T. M. (2022). Generation of PRKN and PINK1-KO and double KO cell lines from healthy induced pluripotent stem cells using CRISPR/Cas9 editing. *BioRxiv*, 2022.02.25.482014. https://doi.org/10.1101/2022.02.25.482014

Choi, B.-K., Choi, M.-G., Kim, J.-Y., Yang, Y., Lai, Y., Kweon, D.-H., Lee, N. K., & Shin, Y.-K. (2013). Large α-synuclein oligomers inhibit neuronal SNARE-mediated vesicle docking. *Proceedings of the National Academy of Sciences*, *110*(10), 4087–4092.

Choi, S. H., Kim, Y. H., Hebisch, M., Sliwinski, C., Lee, S., D'Avanzo, C., Chen, H., Hooli, B., Asselin, C., Muffat, J., Klee, J. B., Zhang, C., Wainger, B. J., Peitz, M., Kovacs, D. M., Woolf, C. J., Wagner, S. L., Tanzi, R. E., & Kim, D. Y. (2014). A three-dimensional human neural cell culture model of Alzheimer's disease. *Nature*, *515*(7526), 274–278. https://doi.org/10.1038/nature13800

Clark, I. E., Dodson, M. W., Jiang, C., Cao, J. H., Huh, J. R., Seol, J. H., Yoo, S. J., Hay, B. A., & Guo, M. (2006). Drosophila pink1 is required for mitochondrial function and interacts genetically with parkin. *Nature*, *441*(7097), 1162–1166. https://doi.org/10.1038/nature04779

Cohen, L. D., Zuchman, R., Sorokina, O., Müller, A., Dieterich, D. C., Armstrong, J. D., Ziv, T., & Ziv, N. E. (2013). Metabolic turnover of synaptic proteins: kinetics, interdependencies and implications for synaptic maintenance. *PloS One*, *8*(5), e63191–e63191. https://doi.org/10.1371/journal.pone.0063191

Cox, J., & Mann, M. (2008). MaxQuant enables high peptide identification rates, individualized p.p.b.-range mass accuracies and proteome-wide protein quantification. *Nature Biotechnology*, *26*(12), 1367–1372. https://doi.org/10.1038/nbt.1511

Cuervo, A. M., Stefanis, L., Fredenburg, R., Lansbury, P. T., & Sulzer, D. (2004). Impaired degradation of mutant α-synuclein by chaperone-mediated autophagy. *Science*, *305*(5688), 1292–1295.

Dakic, V., Minardi Nascimento, J., Costa Sartore, R., Maciel, R. de M., de Araujo, D. B., Ribeiro, S., Martins-de-Souza, D., & Rehen, S. K. (2017). Short term changes in the proteome of human cerebral organoids induced by 5-MeO-DMT. *Scientific Reports*, *7*(1), 12863. https://doi.org/10.1038/s41598-017-12779-5

Dang, J., Tiwari, S. K., Lichinchi, G., Qin, Y., Patil, V. S., Eroshkin, A. M., & Rana, T. M. (2016). Zika virus depletes neural progenitors in human cerebral organoids through activation of the innate immune receptor TLR3. *Cell Stem Cell*, *19*(2), 258–265.

Dauer, W., & Przedborski, S. (2003). Parkinson's Disease: Mechanisms and Models. *Neuron*, *39*(6), 889–909. https://doi.org/10.1016/S0896-6273(03)00568-3

Davies, V., Wandy, J., Weidt, S., van der Hooft, J. J. J., Miller, A., Daly, R., & Rogers, S. (2021). Rapid Development of Improved Data-Dependent Acquisition Strategies. *Analytical Chemistry*, *93*(14), 5676–5683. https://doi.org/10.1021/acs.analchem.0c03895

de Lau, L. M. L., & Breteler, M. M. B. (2006). Epidemiology of Parkinson's disease. *The Lancet Neurology*, *5*(6), 525–535. https://doi.org/https://doi.org/10.1016/S1474-4422(06)70471-9

DeMartino, G. N., & Slaughter, C. A. (1999). The proteasome, a novel protease regulated by multiple mechanisms. *Journal of Biological Chemistry*, *274*(32), 22123–22126.

Dennissen, F. J. A., Kholod, N., & van Leeuwen, F. W. (2012). The ubiquitin proteasome system in neurodegenerative diseases: Culprit, accomplice or victim? *Progress in Neurobiology*, *96*(2), 190–207. https://doi.org/https://doi.org/10.1016/j.pneurobio.2012.01.003

Duan, Y., Li, F., Li, Y., Tang, Y., Kong, X., Feng, Z., Anthony, T. G., Watford, M., Hou, Y., Wu, G., & Yin, Y. (2016). The role of leucine and its metabolites in protein and energy metabolism. *Amino Acids*, *48*(1), 41–51. https://doi.org/10.1007/s00726-015-2067-1

Fatehullah, A., Tan, S. H., & Barker, N. (2016). Organoids as an in vitro model of human development and disease. *Nature Cell Biology*, *18*(3), 246–254. https://doi.org/10.1038/ncb3312

Fecto, F., Esengul, Y. T., & Siddique, T. (2014). Protein recycling pathways in neurodegenerative diseases. *Alzheimer's Research & Therapy*, *6*(2), 13. https://doi.org/10.1186/alzrt243

Fornasiero, E. F., Mandad, S., Wildhagen, H., Alevra, M., Rammner, B., Keihani, S., Opazo, F., Urban, I., Ischebeck, T., Sakib, M. S., Fard, M. K., Kirli, K., Centeno, T. P., Vidal, R. O., Rahman, R.-U., Benito, E., Fischer, A., Dennerlein, S., Rehling, P., … Rizzoli, S. O. (2018). Precisely measured protein lifetimes in the mouse brain reveal differences across tissues and subcellular fractions. *Nature Communications*, *9*(1), 4230. https://doi.org/10.1038/s41467-018-06519-0

Foster, G. L., Schoenheimer, R., & Rittenberg, D. (1939). STUDIES IN PROTEIN METABOLISM: V. THE UTILIZATION OF AMMONIA FOR AMINO ACID AND CREATINE FORMATION IN ANIMALS. *Journal of Biological Chemistry*, *127*(1), 319–327. https://doi.org/https://doi.org/10.1016/S0021-9258(18)73844-1

Friedman, L. G., Lachenmayer, M. L., Wang, J., He, L., Poulose, S. M., Komatsu, M., Holstein, G. R., & Yue, Z. (2012). Disrupted autophagy leads to dopaminergic axon and dendrite degeneration and promotes presynaptic accumulation of α-synuclein and LRRK2 in the brain. *Journal of Neuroscience*, *32*(22), 7585–7593.

Fujioka, S., Ogaki, K., Tacik, P. M., Uitti, R. J., Ross, O. A., & Wszolek, Z. K. (2014). Update on novel familial forms of Parkinson's disease and multiple system atrophy. *Parkinsonism & Related Disorders*, *20*, S29–S34. https://doi.org/https://doi.org/10.1016/S1353-8020(13)70010-5

Ge, P., Dawson, V. L., & Dawson, T. M. (2020). PINK1 and Parkin mitochondrial quality control: a source of regional vulnerability in Parkinson's disease. *Molecular Neurodegeneration*, *15*(1), 20. https://doi.org/10.1186/s13024-020-00367-7

Ge, S. X., Jung, D., & Yao, R. (2020). ShinyGO: a graphical gene-set enrichment tool for animals and plants. *Bioinformatics (Oxford, England)*, *36*(8), 2628–2629. https://doi.org/10.1093/bioinformatics/btz931

Goedhart, J., & Luijsterburg, M. S. (2020). VolcaNoseR is a web app for creating, exploring, labeling and sharing volcano plots. *Scientific Reports*, *10*(1), 20560. https://doi.org/10.1038/s41598-020-76603-3

Gonneaud, A., Jones, C., Turgeon, N., Lévesque, D., Asselin, C., Boudreau, F., & Boisvert, F.-M. (2016). A SILAC-Based Method for Quantitative Proteomic Analysis of Intestinal Organoids. *Scientific Reports*, *6*(1), 38195. https://doi.org/10.1038/srep38195

González-Rodríguez, P., Zampese, E., Stout, K. A., Guzman, J. N., Ilijic, E., Yang, B., Tkatch, T., Stavarache, M. A., Wokosin, D. L., Gao, L., Kaplitt, M. G., López-Barneo, J., Schumacker, P. T., & Surmeier, D. J. (2021). Disruption of mitochondrial complex I induces progressive parkinsonism. *Nature*, *599*(7886), 650–656. https://doi.org/10.1038/s41586-021-04059-0

Greene, J. C., Whitworth, A. J., Kuo, I., Andrews, L. A., Feany, M. B., & Pallanck, L. J. (2003). Mitochondrial pathology and apoptotic muscle degeneration in Drosophila parkin mutants. *Proceedings of the National Academy of Sciences*, *100*(7), 4078–4083. https://doi.org/10.1073/pnas.0737556100

Halperin, A., Elstein, D., & Zimran, A. (2006). Increased incidence of Parkinson disease among relatives of patients with Gaucher disease. *Blood Cells, Molecules, and Diseases*, *36*(3), 426–428. https://doi.org/https://doi.org/10.1016/j.bcmd.2006.02.004

Hanna, J., Guerra-Moreno, A., Ang, J., & Micoogullari, Y. (2018). Protein Degradation and the Pathologic Basis of Disease. *Am J Pathol*, *189*(1), 94–103. https://doi.org/10.1016/j.ajpath.2018.09.004

Heo, S., Diering, G. H., Na, C. H., Nirujogi, R. S., Bachman, J. L., Pandey, A., & Huganir, R. L. (2018). Identification of long-lived synaptic proteins by proteomic analysis of synaptosome protein turnover. *Proceedings of the National Academy of Sciences of the United States of America*, *115*(16), E3827–E3836. https://doi.org/10.1073/pnas.1720956115

Herrmann, J., Ciechanover, A., Lerman, L. O., & Lerman, A. (2004). The ubiquitin-proteasome system in cardiovascular diseases-a hypothesis extended. *Cardiovasc Res*, *61*(1), 11–21. https://doi.org/10.1016/j.cardiores.2003.09.033

Holdorff, B. (2002). Friedrich Heinrich Lewy (1885-1950) and his work. *J Hist Neurosci*, *11*(1), 19–28. https://doi.org/10.1076/jhin.11.1.19.9106

Hsieh, E. J., Shulman, N. J., Dai, D.-F., Vincow, E. S., Karunadharma, P. P., Pallanck, L., Rabinovitch, P. S., & MacCoss, M. J. (2012). Topograph, a software platform for precursor enrichment corrected global protein turnover measurements. *Molecular & Cellular Proteomics : MCP*, *11*(11), 1468–1474. https://doi.org/10.1074/mcp.O112.017699

Iefremova, V., Manikakis, G., Krefft, O., Jabali, A., Weynans, K., Wilkens, R., Marsoner, F., Brändl, B., Müller, F.-J., & Koch, P. (2017). An organoid-based model of cortical development identifies non-cell-autonomous defects in Wnt signaling contributing to Miller-Dieker syndrome. *Cell Reports*, *19*(1), 50–59.

Jo, J., Xiao, Y., Sun, A. X., Cukuroglu, E., Tran, H.-D., Göke, J., Tan, Z. Y., Saw, T. Y., Tan, C.-P., & Lokman, H. (2016). Midbrain-like organoids from human pluripotent stem cells contain functional dopaminergic and neuromelanin-producing neurons. *Cell Stem Cell*, *19*(2), 248–257.

Jo, J., Xiao, Y., Sun, A. X., Cukuroglu, E., Tran, H.-D., Göke, J., Tan, Z. Y., Saw, T. Y., Tan, C.-P., Lokman, H., Lee, Y., Kim, D., Ko, H. S., Kim, S.-O., Park, J. H., Cho, N.-J., Hyde, T. M., Kleinman, J. E., Shin, J. H., … Ng, H.-H. (2016). Midbrain-like Organoids from Human Pluripotent Stem Cells Contain Functional Dopaminergic and Neuromelanin-Producing Neurons. *Cell Stem Cell*, *19*(2), 248–257. https://doi.org/10.1016/j.stem.2016.07.005

Kane, L. A., & Youle, R. J. (2011). PINK1 and Parkin Flag Miro to Direct Mitochondrial Traffic. *Cell*, *147*(4), 721–723. https://doi.org/10.1016/j.cell.2011.10.028

Kanehisa, M., & Goto, S. (2000). KEGG: Kyoto Encyclopedia of Genes and Genomes. *Nucleic Acids Research*, *28*(1), 27–30. https://doi.org/10.1093/nar/28.1.27

Karbowski, M., & Neutzner, A. (2012). Neurodegeneration as a consequence of failed mitochondrial maintenance. *Acta Neuropathologica*, *123*(2), 157–171. https://doi.org/10.1007/s00401-011-0921-0

Kelava, I., & Lancaster, M. A. (2016). Stem Cell Models of Human Brain Development. *Cell Stem Cell*, *18*(6), 736–748. https://doi.org/10.1016/j.stem.2016.05.022

Keller, J. N., Hanni, K. B., & Markesbery, W. R. (2000). Impaired proteasome function in Alzheimer's disease. *Journal of Neurochemistry*, *75*(1), 436–439.

Kelly, R. T. (2020). Single-cell Proteomics: Progress and Prospects. *Molecular & Cellular Proteomics*, *19*(11), 1739–1748. https://doi.org/10.1074/mcp.R120.002234

Kim, M.-S., Pinto, S. M., Getnet, D., Nirujogi, R. S., Manda, S. S., Chaerkady, R., Madugundu, A. K., Kelkar, D. S., Isserlin, R., Jain, S., Thomas, J. K., Muthusamy, B., Leal-Rojas, P., Kumar, P., Sahasrabuddhe, N. A., Balakrishnan, L., Advani, J., George, B., Renuse, S., … Pandey, A. (2014). A draft map of the human proteome. *Nature*, *509*(7502), 575–581. https://doi.org/10.1038/nature13302

Konno, T., Ross, O. A., Puschmann, A., Dickson, D. W., & Wszolek, Z. K. (2016). Autosomal dominant Parkinson's disease caused by SNCA duplications. *Parkinsonism & Related Disorders*, *22*, S1–S6. https://doi.org/https://doi.org/10.1016/j.parkreldis.2015.09.007

Konvalinka, A., Zhou, J., Dimitromanolakis, A., Drabovich, A. P., Fang, F., Gurley, S., Coffman, T., John, R., Zhang, S.-L., Diamandis, E. P., & Scholey, J. W. (2013). Determination of an Angiotensin II-regulated Proteome in Primary Human Kidney Cells by Stable Isotope Labeling of Amino Acids in Cell Culture (SILAC) . *Journal of Biological Chemistry*, *288*(34), 24834–24847. https://doi.org/10.1074/jbc.M113.485326

Krüger, M., Moser, M., Ussar, S., Thievessen, I., Luber, C. A., Forner, F., Schmidt, S., Zanivan, S., Fässler, R., & Mann, M. (2008). SILAC Mouse for Quantitative Proteomics Uncovers Kindlin-3 as an Essential Factor for Red Blood Cell Function. *Cell*, *134*(2), 353–364. https://doi.org/10.1016/j.cell.2008.05.033

Lammel, S., Lim, B. K., Ran, C., Huang, K. W., Betley, M. J., Tye, K. M., Deisseroth, K., & Malenka, R. C. (2012). Input-specific control of reward and aversion in the ventral tegmental area. *Nature*, *491*(7423), 212–217. https://doi.org/10.1038/nature11527

Lancaster, M. A., Renner, M., Martin, C.-A., Wenzel, D., Bicknell, L. S., Hurles, M. E., Homfray, T., Penninger, J. M., Jackson, A. P., & Knoblich, J. A. (2013). Cerebral

organoids model human brain development and microcephaly. *Nature*, *501*(7467), 373–379. https://doi.org/10.1038/nature12517

Langston, J. W., Ballard, P., Tetrud, J. W., & Irwin, I. (1983). Chronic Parkinsonism in Humans Due to a Product of Meperidine-Analog Synthesis. *Science*, *219*(4587), 979–980. https://doi.org/10.1126/science.6823561

Lee, J. J., Sanchez-Martinez, A., Martinez Zarate, A., Benincá, C., Mayor, U., Clague, M. J., & Whitworth, A. J. (2018). Basal mitophagy is widespread in Drosophila but minimally affected by loss of Pink1 or parkin. *The Journal of Cell Biology*, *217*(5), 1613–1622. https://doi.org/10.1083/jcb.201801044

Lee, J. J., Sanchez-Martinez, A., Zarate, A. M., Benincá, C., Mayor, U., Clague, M. J., & Whitworth, A. J. (2018). Basal mitophagy is widespread in Drosophila but minimally affected by loss of Pink1 or parkin. *Journal of Cell Biology*, *217*(5), 1613–1622. https://doi.org/10.1083/jcb.201801044

Lehman, N. L. (2009). The ubiquitin proteasome system in neuropathology. *Acta Neuropathol*, *118*(3), 329–347. https://doi.org/10.1007/s00401-009-0560-x

Lill, C. M. (2016). Genetics of Parkinson's disease. *Molecular and Cellular Probes*, *30*(6), 386–396. https://doi.org/https://doi.org/10.1016/j.mcp.2016.11.001

Lindersson, E., Beedholm, R., Højrup, P., Moos, T., Gai, W., Hendil, K. B., & Jensen, P. H. (2004). Proteasomal inhibition by α-synuclein filaments and oligomers. *Journal of Biological Chemistry*, *279*(13), 12924–12934.

Liu, H., Sadygov, R. G., & Yates, J. R. (2004). A model for random sampling and estimation of relative protein abundance in shotgun proteomics. *Analytical Chemistry*, *76*(14), 4193–4201.

Liu, Y.-T., Sliter, D. A., Shammas, M. K., Huang, X., Wang, C., Calvelli, H., Maric, D. S., & Narendra, D. P. (2021). Mt-Keima detects PINK1-PRKN mitophagy in vivo with greater sensitivity than mito-QC. *Autophagy*, *17*(11), 3753–3762. https://doi.org/10.1080/15548627.2021.1896924

Looso, M., Borchardt, T., Krüger, M., & Braun, T. (2010). Advanced identification of proteins in uncharacterized proteomes by pulsed in vivo stable isotope labeling-based mass spectrometry. *Molecular & Cellular Proteomics : MCP*, *9*(6), 1157–1166. https://doi.org/10.1074/mcp.M900426-MCP200

MacLean, B., Tomazela, D. M., Shulman, N., Chambers, M., Finney, G. L., Frewen, B., Kern, R., Tabb, D. L., Liebler, D. C., & MacCoss, M. J. (2010). Skyline: an open source document editor for creating and analyzing targeted proteomics experiments. *Bioinformatics (Oxford, England)*, *26*(7), 966–968. https://doi.org/10.1093/bioinformatics/btq054

Mariani, J., Coppola, G., Zhang, P., Abyzov, A., Provini, L., Tomasini, L., Amenduni, M., Szekely, A., Palejev, D., & Wilson, M. (2015). FOXG1-dependent dysregulation of GABA/glutamate neuron differentiation in autism spectrum disorders. *Cell*, *162*(2), 375–390.

Martin, L. J., Pan, Y., Price, A. C., Sterling, W., Copeland, N. G., Jenkins, N. A., Price, D. L., & Lee, M. K. (2006). Parkinson's disease α-synuclein transgenic mice develop neuronal mitochondrial degeneration and cell death. *Journal of Neuroscience*, *26*(1), 41–50.

Martinez-Vicente, M., Talloczy, Z., Kaushik, S., Massey, A. C., Mazzulli, J., Mosharov, E. v, Hodara, R., Fredenburg, R., Wu, D.-C., & Follenzi, A. (2008). Dopamine-modified α-synuclein blocks chaperone-mediated autophagy. *The Journal of Clinical Investigation*, *118*(2), 777–788.

Martinez-Zapien, D., Ruiz, F. X., Poirson, J., Mitschler, A., Ramirez, J., Forster, A., Cousido-Siah, A., Masson, M., Pol, S. vande, Podjarny, A., Travé, G., & Zanier, K. (2016). Structure of the E6/E6AP/p53 complex required for HPV-mediated degradation of p53. *Nature*, *529*(7587), 541–545. https://doi.org/10.1038/nature16481

Matheoud, D., Cannon, T., Voisin, A., Penttinen, A.-M., Ramet, L., Fahmy, A. M., Ducrot, C., Laplante, A., Bourque, M.-J., Zhu, L., Cayrol, R., le Campion, A., McBride, H. M., Gruenheid, S., Trudeau, L.-E., & Desjardins, M. (2019). Intestinal infection triggers Parkinson's disease-like symptoms in Pink1−/− mice. *Nature*, *571*(7766), 565–569. https://doi.org/10.1038/s41586-019-1405-y

Matsuda, W., Furuta, T., Nakamura, K. C., Hioki, H., Fujiyama, F., Arai, R., & Kaneko, T. (2009). Single Nigrostriatal Dopaminergic Neurons Form Widely Spread and Highly Dense Axonal Arborizations in the Neostriatum. *The Journal of Neuroscience*, *29*(2), 444. https://doi.org/10.1523/JNEUROSCI.4029-08.2009

Mazzulli, J. R., Xu, Y.-H., Sun, Y., Knight, A. L., McLean, P. J., Caldwell, G. A., Sidransky, E., Grabowski, G. A., & Krainc, D. (2011). Gaucher disease glucocerebrosidase and α-synuclein form a bidirectional pathogenic loop in synucleinopathies. *Cell*, *146*(1), 37–52.

McLelland, G., Soubannier, V., Chen, C. X., McBride, H. M., & Fon, E. A. (2014). Parkin and PINK 1 function in a vesicular trafficking pathway regulating mitochondrial quality control. *The EMBO Journal*, *33*(4), 282–295.

McLelland, G.-L., Soubannier, V., Chen, C. X., McBride, H. M., & Fon, E. A. (2014). Parkin and PINK1 function in a vesicular trafficking pathway regulating mitochondrial quality control. *The EMBO Journal*, *33*(4), 282–295. https://doi.org/https://doi.org/10.1002/embj.201385902

McWilliams, T. G., Prescott, A. R., Allen, G. F. G., Tamjar, J., Munson, M. J., Thomson, C., Muqit, M. M. K., & Ganley, I. G. (2016). mito-QC illuminates mitophagy and mitochondrial architecture in vivo. *Journal of Cell Biology*, *214*(3), 333–345. https://doi.org/10.1083/jcb.201603039

McWilliams, T. G., Prescott, A. R., Montava-Garriga, L., Ball, G., Singh, F., Barini, E., Muqit, M. M. K., Brooks, S. P., & Ganley, I. G. (2018a). Basal Mitophagy Occurs Independently of PINK1 in Mouse Tissues of High Metabolic Demand. *Cell Metab*, *27*(2), 439-449.e5. https://doi.org/10.1016/j.cmet.2017.12.008

McWilliams, T. G., Prescott, A. R., Montava-Garriga, L., Ball, G., Singh, F., Barini, E., Muqit, M. M. K., Brooks, S. P., & Ganley, I. G. (2018b). Basal Mitophagy Occurs Independently of PINK1 in Mouse Tissues of High Metabolic Demand. *Cell Metabolism*, *27*(2), 439-449.e5. https://doi.org/10.1016/j.cmet.2017.12.008

Mohamed, N.-V., Lépine, P., Lacalle-Aurioles, M., Sirois, J., Mathur, M., Reintsch, W., Beitel, L. K., Fon, E. A., & Durcan, T. M. (2021). Microfabricated disk technology: Rapid scale up in midbrain organoid generation. *Methods*. https://doi.org/10.1016/J.YMETH.2021.07.008

Mohamed, N.-V., Mathur, M., da Silva, R. v, Thomas, R. A., Lepine, P., Beitel, L. K., Fon, E. A., & Durcan, T. M. (2021). Generation of human midbrain organoids from induced pluripotent stem cells. *MNI Open Research*, *3*, 1.

Mohamed, N.-V., Sirois, J., Ramamurthy, J., Mathur, M., Lépine, P., Deneault, E., Maussion, G., Nicouleau, M., Chen, C. X.-Q., Abdian, N., Soubannier, V., Cai, E., Nami, H., Thomas, R. A., Wen, D., Tabatabaei, M., Beitel, L. K., Singh Dolt, K., Karamchandani, J., … Durcan, T. M. (2021a). Midbrain organoids with an SNCA gene triplication model key features of synucleinopathy. *Brain Communications*. https://doi.org/10.1093/braincomms/fcab223

Mohamed, N.-V., Sirois, J., Ramamurthy, J., Mathur, M., Lépine, P., Deneault, E., Maussion, G., Nicouleau, M., Chen, C. X.-Q., Abdian, N., Soubannier, V., Cai, E., Nami, H., Thomas, R. A., Wen, D., Tabatabaei, M., Beitel, L. K., Singh Dolt, K., Karamchandani, J., … Durcan, T. M. (2021b). Midbrain organoids with an SNCA gene triplication model key features of synucleinopathy. *Brain Communications*, *3*(4), fcab223. https://doi.org/10.1093/braincomms/fcab223

Mohamed, N. v, Mathur, M., da Silva, R. v, Thomas, R. A., Lepine, P., Beitel, L. K., Fon, E. A., & Durcan, T. M. (2021). Generation of human midbrain organoids from induced pluripotent stem cells [version 2; peer review: 3 approved, 1 approved with reservations] . *MNI Open Research*, *3*(1). https://doi.org/10.12688/mniopenres.12816.2

Mortiboys, H., Thomas, K. J., Koopman, W. J. H., Klaffke, S., Abou-Sleiman, P., Olpin, S., Wood, N. W., Willems, P. H. G. M., Smeitink, J. A. M., Cookson, M. R., & Bandmann, O. (2008). Mitochondrial function and morphology are impaired in parkin-mutant fibroblasts. *Annals of Neurology*, *64*(5), 555–565. https://doi.org/https://doi.org/10.1002/ana.21492

Narendra, D. P., & Youle, R. J. (2011). Targeting mitochondrial dysfunction: role for PINK1 and Parkin in mitochondrial quality control. *Antioxidants & Redox Signaling*, *14*(10), 1929–1938. https://doi.org/10.1089/ars.2010.3799

Nemani, V. M., Lu, W., Berge, V., Nakamura, K., Onoa, B., Lee, M. K., Chaudhry, F. A., Nicoll, R. A., & Edwards, R. H. (2010). Increased expression of α-synuclein reduces neurotransmitter release by inhibiting synaptic vesicle reclustering after endocytosis. *Neuron*, *65*(1), 66–79.

Nemchenko, A., Chiong, M., Turer, A., Lavandero, S., & Hill, J. A. (2011). Autophagy as a therapeutic target in cardiovascular disease. *Journal of Molecular and Cellular*

Cardiology, *51*(4), 584–593. https://doi.org/https://doi.org/10.1016/j.yjmcc.2011.06.010

Nixon, R. A. (2013). The role of autophagy in neurodegenerative disease. *Nature Medicine*, *19*(8), 983–997. https://doi.org/10.1038/nm.3232

Notaras, M., Lodhi, A., Barrio-Alonso, E., Foord, C., Rodrick, T., Jones, D., Fang, H., Greening, D., & Colak, D. (2021). Neurodevelopmental signatures of narcotic and neuropsychiatric risk factors in 3D human-derived forebrain organoids. *Molecular Psychiatry*. https://doi.org/10.1038/s41380-021-01189-9

Ong, S.-E., Kratchmarova, I., & Mann, M. (2003). Properties of 13C-Substituted Arginine in Stable Isotope Labeling by Amino Acids in Cell Culture (SILAC). *Journal of Proteome Research*, *2*(2), 173–181. https://doi.org/10.1021/pr0255708

Ong, S.-E., & Mann, M. (2005). Mass spectrometry–based proteomics turns quantitative. *Nature Chemical Biology*, *1*(5), 252–262. https://doi.org/10.1038/nchembio736

Palacino, J. J., Sagi, D., Goldberg, M. S., Krauss, S., Motz, C., Wacker, M., Klose, J., & Shen, J. (2004). Mitochondrial Dysfunction and Oxidative Damage in parkin-deficient Mice *. *Journal of Biological Chemistry*, *279*(18), 18614–18622. https://doi.org/10.1074/jbc.M401135200

Parkinson's Disease: Pathogenesis and Clinical Aspects. (2018). Codon Publications. https://doi.org/10.15586/codonpublications.parkinsonsdisease.2018

Patron, M., Tarasenko, D., Nolte, H., Kroczek, L., Ghosh, M., Ohba, Y., Lasarzewski, Y., Ahmadi, Z. A., Cabrera-Orefice, A., Eyiama, A., Kellermann, T., Rugarli, E. I., Brandt, U., Meinecke, M., & Langer, T. (2022). Regulation of mitochondrial proteostasis by the proton gradient. *The EMBO Journal*, *41*(16), e110476. https://doi.org/https://doi.org/10.15252/embj.2021110476

Perez-Riverol, Y., Bai, J., Bandla, C., García-Seisdedos, D., Hewapathirana, S., Kamatchinathan, S., Kundu, D. J., Prakash, A., Frericks-Zipper, A., Eisenacher, M., Walzer, M., Wang, S., Brazma, A., & Vizcaíno, J. A. (2022). The PRIDE database resources in 2022: a hub for mass spectrometry-based proteomics evidences. *Nucleic Acids Research*, *50*(D1), D543–D552. https://doi.org/10.1093/nar/gkab1038

Pickrell, A. M., Huang, C.-H., Kennedy, S. R., Ordureau, A., Sideris, D. P., Hoekstra, J. G., Harper, J. W., & Youle, R. J. (2015). Endogenous Parkin preserves dopaminergic substantia nigral neurons following mitochondrial DNA mutagenic stress. *Neuron*, *87*(2), 371–381.

Pickrell, A. M., & Youle, R. J. (2015). The roles of PINK1, parkin, and mitochondrial fidelity in Parkinson's disease. *Neuron*, *85*(2), 257–273.

Picotti, P., & Aebersold, R. (2012). Selected reaction monitoring–based proteomics: workflows, potential, pitfalls and future directions. *Nature Methods*, *9*(6), 555–566. https://doi.org/10.1038/nmeth.2015

Polymeropoulos, M. H., Lavedan, C., Leroy, E., Ide, S. E., Dehejia, A., Dutra, A., Pike, B., Root, H., Rubenstein, J., Boyer, R., Stenroos, E. S., Chandrasekharappa, S., Athanassiadou, A., Papapetropoulos, T., Johnson, W. G., Lazzarini, A. M., Duvoisin, R. C., di Iorio, G., Golbe, L. I., & Nussbaum, R. L. (1997). Mutation in the alpha-synuclein gene identified in families with Parkinson's disease. *Science*, *276*(5321), 2045–2047. https://doi.org/10.1126/science.276.5321.2045

Price, J. C., Guan, S., Burlingame, A., Prusiner, S. B., & Ghaemmaghami, S. (2010). Analysis of proteome dynamics in the mouse brain. *Proceedings of the National Academy of Sciences of the United States of America*, *107*(32), 14508–14513. https://doi.org/10.1073/pnas.1006551107

Pryde, K. R., Smith, H. L., Chau, K.-Y., & Schapira, A. H. v. (2016). PINK1 disables the anti-fission machinery to segregate damaged mitochondria for mitophagy. *Journal of Cell Biology*, *213*(2), 163–171.

Qian, X., Song, H., & Ming, G. (2019). Brain organoids: advances, applications and challenges. *Development*, *146*(8), dev166074. https://doi.org/10.1242/dev.166074

Raja, W. K., Mungenast, A. E., Lin, Y.-T., Ko, T., Abdurrob, F., Seo, J., & Tsai, L.-H. (2016). Self-organizing 3D human neural tissue derived from induced pluripotent stem cells recapitulate Alzheimer's disease phenotypes. *PloS One*, *11*(9), e0161969.

Rauniyar, N., & Yates 3rd, J. R. (2014). Isobaric labeling-based relative quantification in shotgun proteomics. *J Proteome Res*, *13*(12), 5293–5309. https://doi.org/10.1021/pr500880b

Roberts, R. F., Bayne, A. N., Goiran, T., Lévesque, D., Boisvert, F.-M., Trempe, J.-F., & Fon, E. A. (2020). Proteomic profiling of mitochondrial-derived vesicles in brain reveals enrichment of respiratory complex sub-assemblies and small TIM chaperones. *Journal of Proteome Research*, *20*(1), 506–517.

Rosenbloom, B. E., & Weinreb, N. J. (2013). Gaucher disease: a comprehensive review. *Critical Reviews™ in Oncogenesis*, *18*(3).

Ryan, B. J., Hoek, S., Fon, E. A., & Wade-Martins, R. (2015). Mitochondrial dysfunction and mitophagy in Parkinson's: from familial to sporadic disease. *Trends in Biochemical Sciences*, *40*(4), 200–210. https://doi.org/https://doi.org/10.1016/j.tibs.2015.02.003

Salcedo, C., Andersen, J. v, Vinten, K. T., Pinborg, L. H., Waagepetersen, H. S., Freude, K. K., & Aldana, B. I. (2021). Functional Metabolic Mapping Reveals Highly Active Branched-Chain Amino Acid Metabolism in Human Astrocytes, Which Is Impaired in iPSC-Derived Astrocytes in Alzheimer's Disease. *Front Aging Neurosci*, *13*, 736580. https://doi.org/10.3389/fnagi.2021.736580

Sato, S., Uchihara, T., Fukuda, T., Noda, S., Kondo, H., Saiki, S., Komatsu, M., Uchiyama, Y., Tanaka, K., & Hattori, N. (2018). Loss of autophagy in dopaminergic neurons causes Lewy pathology and motor dysfunction in aged mice. *Scientific Reports*, *8*(1), 1–10.

Scheffner, M., Huibregtse, J. M., Vierstra, R. D., & Howley, P. M. (1993). The HPV-16 E6 and E6-AP complex functions as a ubiquitin-protein ligase in the ubiquitination of p53. *Cell*, *75*(3), 495–505. https://doi.org/https://doi.org/10.1016/0092-8674(93)90384-3

Scott, D. A., Tabarean, I., Tang, Y., Cartier, A., Masliah, E., & Roy, S. (2010). A Pathologic Cascade Leading to Synaptic Dysfunction in α-Synuclein-Induced Neurodegeneration. *The Journal of Neuroscience*, *30*(24), 8083. https://doi.org/10.1523/JNEUROSCI.1091-10.2010

Shahmoradian, S. H., Lewis, A. J., Genoud, C., Hench, J., Moors, T. E., Navarro, P. P., Castaño-Díez, D., Schweighauser, G., Graff-Meyer, A., Goldie, K. N., Sütterlin, R., Huisman, E., Ingrassia, A., Gier, Y. de, Rozemuller, A. J. M., Wang, J., Paepe, A. de, Erny, J., Staempfli, A., … Lauer, M. E. (2019). Lewy pathology in Parkinson's

disease consists of crowded organelles and lipid membranes. *Nature Neuroscience*, *22*(7), 1099–1109. https://doi.org/10.1038/s41593-019-0423-2

Sherer, T. B., Betarbet, R., Testa, C. M., Seo, B. B., Richardson, J. R., Kim, J. H., Miller, G. W., Yagi, T., Matsuno-Yagi, A., & Greenamyre, J. T. (2003). Mechanism of Toxicity in Rotenone Models of Parkinson's Disease. *The Journal of Neuroscience*, *23*(34), 10756. https://doi.org/10.1523/JNEUROSCI.23-34-10756.2003

Shevchenko, A., Tomas, H., Havli, J., Olsen, J. v, & Mann, M. (2006). In-gel digestion for mass spectrometric characterization of proteins and proteomes. *Nature Protocols*, *1*(6), 2856–2860. https://doi.org/10.1038/nprot.2006.468

Shoffner, J. M., Watts, R. L., Juncos, J. L., Torroni, A., & Wallace, D. C. (1991). Mitochondrial oxidative phosphorylation defects in parkinson's disease. *Annals of Neurology*, *30*(3), 332–339. https://doi.org/https://doi.org/10.1002/ana.410300304

Smith, L., & Schapira, A. H. v. (2022). GBA Variants and Parkinson Disease: Mechanisms and Treatments. *Cells*, *11*(8). https://doi.org/10.3390/cells11081261

Snyder, H., Mensah, K., Theisler, C., Lee, J., Matouschek, A., & Wolozin, B. (2003). Aggregated and monomeric α-synuclein bind to the S6′ proteasomal protein and inhibit proteasomal function. *Journal of Biological Chemistry*, *278*(14), 11753–11759.

Son, J. H., Shim, J. H., Kim, K.-H., Ha, J.-Y., & Han, J. Y. (2012). Neuronal autophagy and neurodegenerative diseases. *Experimental & Molecular Medicine*, *44*(2), 89–98. https://doi.org/10.3858/emm.2012.44.2.031

Soubannier, V., McLelland, G.-L., Zunino, R., Braschi, E., Rippstein, P., Fon, E. A., & McBride, H. M. (2012). A vesicular transport pathway shuttles cargo from mitochondria to lysosomes. *Curr Biol*, *22*(2), 135–141. https://doi.org/10.1016/j.cub.2011.11.057

Stefanis, L. (2012). α-Synuclein in Parkinson's disease. *Cold Spring Harb Perspect Med*, *2*(2), a009399. https://doi.org/10.1101/cshperspect.a009399

Sugiura, A., McLelland, G.-L., Fon, E. A., & McBride, H. M. (2014). A new pathway for mitochondrial quality control: mitochondrial-derived vesicles. *The EMBO Journal*, *33*(19), 2142–2156. https://doi.org/https://doi.org/10.15252/embj.201488104

Sun, N., Yun, J., Liu, J., Malide, D., Liu, C., Rovira, I. I., Holmström, K. M., Fergusson, M. M., Yoo, Y. H., Combs, C. A., & Finkel, T. (2015a). Measuring In Vivo Mitophagy. *Mol Cell*, *60*(4), 685–696. https://doi.org/10.1016/j.molcel.2015.10.009

Sun, N., Yun, J., Liu, J., Malide, D., Liu, C., Rovira, I. I., Holmström, K. M., Fergusson, M. M., Yoo, Y. H., Combs, C. A., & Finkel, T. (2015b). Measuring In Vivo Mitophagy. *Mol Cell*, *60*(4), 685–696. https://doi.org/10.1016/j.molcel.2015.10.009

Surmeier, D. J. (2007). Calcium, ageing, and neuronal vulnerability in Parkinson's disease. *The Lancet Neurology*, *6*(10), 933–938. https://doi.org/https://doi.org/10.1016/S1474-4422(07)70246-6

Surmeier, D. J., Schumacker, P. T., Guzman, J. D., Ilijic, E., Yang, B., & Zampese, E. (2017). Calcium and Parkinson's disease. *Biochemical and Biophysical Research Communications*, *483*(4), 1013–1019. https://doi.org/https://doi.org/10.1016/j.bbrc.2016.08.168

Szklarczyk, D., Gable, A. L., Lyon, D., Junge, A., Wyder, S., Huerta-Cepas, J., Simonovic, M., Doncheva, N. T., Morris, J. H., Bork, P., Jensen, L. J., & Mering, C. von. (2019). STRING v11: protein-protein association networks with increased coverage, supporting functional discovery in genome-wide experimental datasets. *Nucleic Acids Research*, *47*(D1), D607–D613. https://doi.org/10.1093/nar/gky1131

Tabb, D. L., Vega-Montoto, L., Rudnick, P. A., Variyath, A. M., Ham, A.-J. L., Bunk, D. M., Kilpatrick, L. E., Billheimer, D. D., Blackman, R. K., Cardasis, H. L., Carr, S. A., Clauser, K. R., Jaffe, J. D., Kowalski, K. A., Neubert, T. A., Regnier, F. E., Schilling, B., Tegeler, T. J., Wang, M., … Spiegelman, C. (2010). Repeatability and Reproducibility in Proteomic Identifications by Liquid Chromatography−Tandem Mass Spectrometry. *Journal of Proteome Research*, *9*(2), 761–776. https://doi.org/10.1021/pr9006365

Takebe, T., & Wells, J. M. (2019). Organoids by design. *Science*, *364*(6444), 956–959. https://doi.org/10.1126/science.aaw7567

Tanaka, A., Cleland, M. M., Xu, S., Narendra, D. P., Suen, D.-F., Karbowski, M., & Youle, R. J. (2010). Proteasome and p97 mediate mitophagy and degradation of mitofusins induced by Parkin. *Journal of Cell Biology*, *191*(7), 1367–1380.

Tolkovsky, A. M. (2009). Mitophagy. *Biochimica et Biophysica Acta (BBA) - Molecular Cell Research*, *1793*(9), 1508–1515. https://doi.org/https://doi.org/10.1016/j.bbamcr.2009.03.002

Tolosa, E., Vila, M., Klein, C., & Rascol, O. (2020). LRRK2 in Parkinson disease: challenges of clinical trials. *Nature Reviews Neurology*, *16*(2), 97–107.

Toyama, B. H., Savas, J. N., Park, S. K., Harris, M. S., Ingolia, N. T., Yates III, J. R., & Hetzer, M. W. (2013). Identification of Long-Lived Proteins Reveals Exceptional Stability of Essential Cellular Structures. *Cell*, *154*(5), 971–982. https://doi.org/10.1016/j.cell.2013.07.037

Trifunovic, A., Wredenberg, A., Falkenberg, M., Spelbrink, J. N., Rovio, A. T., Bruder, C. E., Bohlooly-Y, M., Gidlöf, S., Oldfors, A., Wibom, R., Törnell, J., Jacobs, H. T., & Larsson, N.-G. (2004). Premature ageing in mice expressing defective mitochondrial DNA polymerase. *Nature*, *429*(6990), 417–423. https://doi.org/10.1038/nature02517

Tysnes, O.-B., & Storstein, A. (2017). Epidemiology of Parkinson's disease. *Journal of Neural Transmission*, *124*(8), 901–905. https://doi.org/10.1007/s00702-017-1686-y

Velasco, V., Shariati, S. A., & Esfandyarpour, R. (2020). Microtechnology-based methods for organoid models. *Microsystems & Nanoengineering*, *6*(1), 76. https://doi.org/10.1038/s41378-020-00185-3

Vidova, V., & Spacil, Z. (2017). A review on mass spectrometry-based quantitative proteomics: Targeted and data independent acquisition. *Analytica Chimica Acta*, *964*, 7–23. https://doi.org/https://doi.org/10.1016/j.aca.2017.01.059

Vincow, E. S., Merrihew, G., Thomas, R. E., Shulman, N. J., Beyer, R. P., MacCoss, M. J., & Pallanck, L. J. (2013a). The PINK1–Parkin pathway promotes both mitophagy and selective respiratory chain turnover in vivo. *Proceedings of the National Academy of Sciences*, *110*(16), 6400–6405. https://doi.org/10.1073/pnas.1221132110

Vincow, E. S., Merrihew, G., Thomas, R. E., Shulman, N. J., Beyer, R. P., MacCoss, M. J., & Pallanck, L. J. (2013b). The PINK1-Parkin pathway promotes both mitophagy and selective respiratory chain turnover in vivo. *Proceedings of the National*

Academy of Sciences of the United States of America, *110*(16), 6400–6405. https://doi.org/10.1073/pnas.1221132110

Welle, K. A., Zhang, T., Hryhorenko, J. R., Shen, S., Qu, J., & Ghaemmaghami, S. (2016). Time-resolved Analysis of Proteome Dynamics by Tandem Mass Tags and Stable Isotope Labeling in Cell Culture (TMT-SILAC) Hyperplexing. *Mol Cell Proteomics*, *15*(12), 3551–3563. https://doi.org/10.1074/mcp.M116.063230

Westman-Brinkmalm, A., Abramsson, A., Pannee, J., Gang, C., Gustavsson, M. K., von Otter, M., Blennow, K., Brinkmalm, G., Heumann, H., & Zetterberg, H. (2011). SILAC zebrafish for quantitative analysis of protein turnover and tissue regeneration. *Journal of Proteomics*, *75*(2), 425–434. https://doi.org/https://doi.org/10.1016/j.jprot.2011.08.008

White, E. (2015). The role for autophagy in cancer. *The Journal of Clinical Investigation*, *125*(1), 42–46. https://doi.org/10.1172/JCI73941

Whitworth, A. J., & Pallanck, L. J. (2017). PINK1/Parkin mitophagy and neurodegeneration—what do we really know in vivo? *Current Opinion in Genetics & Development*, *44*, 47–53. https://doi.org/https://doi.org/10.1016/j.gde.2017.01.016

Winslow, A. R., Chen, C.-W., Corrochano, S., Acevedo-Arozena, A., Gordon, D. E., Peden, A. A., Lichtenberg, M., Menzies, F. M., Ravikumar, B., & Imarisio, S. (2010). α-Synuclein impairs macroautophagy: implications for Parkinson's disease. *Journal of Cell Biology*, *190*(6), 1023–1037.

Wrighton, P. J., Shwartz, A., Heo, J.-M., Quenzer, E. D., LaBella, K. A., Harper, J. W., & Goessling, W. (2021). Quantitative intravital imaging in zebrafish reveals in vivo dynamics of physiological-stress-induced mitophagy. *Journal of Cell Science*, *134*(4), jcs256255. https://doi.org/10.1242/jcs.256255

X.-Q. Chen, C., Deneault, E., Abdian, N., You, Z., Sirois, J., Nicouleau, M., Shlaifer, I., Villegas, L., Boivin, M.-N., Gaborieau, L., Karamchandani, J., Beitel, L. K., Fon, E. A., & Durcan, T. M. (2022). Generation of patient-derived pluripotent stem cell-lines and CRISPR modified isogenic controls with mutations in the Parkinson's associated GBA gene. *Stem Cell Research*, *64*, 102919. https://doi.org/https://doi.org/10.1016/j.scr.2022.102919

Xu, L., & Pu, J. (2016). Alpha-Synuclein in Parkinson's Disease: From Pathogenetic Dysfunction to Potential Clinical Application. *Parkinson's Disease*, *2016*, 1720621. https://doi.org/10.1155/2016/1720621

Yang, R., Gao, G., Mao, Z., & Yang, Q. (2016). Chaperone-Mediated Autophagy and Mitochondrial Homeostasis in Parkinson's Disease. *Parkinsons Dis*, *2016*, 2613401. https://doi.org/10.1155/2016/2613401

Zhang, L., & Elias, J. E. (2017). Relative Protein Quantification Using Tandem Mass Tag Mass Spectrometry. In L. Comai, J. E. Katz, & P. Mallick (Eds.), *Proteomics: Methods and Protocols* (pp. 185–198). Springer New York. https://doi.org/10.1007/978-1-4939-6747-6_14

Zhao, X., Xu, Z., Xiao, L., Shi, T., Xiao, H., Wang, Y., Li, Y., Xue, F., & Zeng, W. (2021). Review on the Vascularization of Organoids and Organoids-on-a-Chip. *Frontiers in Bioengineering and Biotechnology*, *9*, 223. https://doi.org/10.3389/fbioe.2021.637048

Ziviani, E., Tao, R. N., & Whitworth, A. J. (2010). Drosophila parkin requires PINK1 for mitochondrial translocation and ubiquitinates mitofusin. *Proceedings of the National Academy of Sciences*, *107*(11), 5018–5023.

McGill

Co-author permission for use of published or in-preparation manuscripts:

I, Anthony Duchesne, consent to the incorporation of the following materials in the Master's thesis prepared by Jing Dong.

Dong, J., Duchesne, A., Bayne, A. N., Mohamed, N. V., Yi, W., Mathur, M., Chen, C., You, Z., Abdian, N., Taylor, L., Fon, E. A., Durcan, T. M., & Trempe, J. F. (2022). An approach to measuring protein turnover in human induced pluripotent stem cell organoids by mass spectrometry. Methods (San Diego, Calif.), 203, 17–27. https://doi.org/10.1016/j.ymeth.2022.03.011

Anthony Duchesne
November 1st, 2022

McGill

Co-author permission for use of published or in-preparation manuscripts:

I Andrew Bayne consent to the incorporation of the following materials in the Master's thesis prepared by Jing Dong.

Dong, J., Duchesne, A., Bayne, A. N., Mohamed, N. V., Yi, W., Mathur, M., Chen, C., You, Z., Abdian, N., Taylor, L., Fon, E. A., Durcan, T. M., & Trempe, J. F. (2022). An approach to measuring protein turnover in human induced pluripotent stem cell organoids by mass spectrometry. Methods (San Diego, Calif.), 203, 17–27. https://doi.org/10.1016/j.ymeth.2022.03.011

Signature 

Date: November 1st 2022